JPET Fast Forward. Published on October 12, 2006 as DOI: 10.1124/jpet.106.107433

JPET #107433

Bias in Estimation of Transporter Kinetic Parameters from Over-expression Systems: Interplay of Transporter Expression Level and Substrate Affinity

Anand Balakrishnan[1], Naissan Hussainzada, Pablo Gonzalez, Marival Bermejo, Peter W. Swaan, and James E. Polli

Department of Pharmaceutical Sciences, School of Pharmacy, University of Maryland, Baltimore, Maryland (A.B., N.H., P.G., P.W.S., J.E.P.); and Department of Pharmacy and Technology, University of Valencia, Valencia, Spain (M.B.)

Running Title : ABL Influence on Transporter Kinetics

Corresponding Author :

James E. Polli, Department of Pharmaceutical Sciences, School of Pharmacy, University of Maryland, 20 Penn Street, HSF2 room 623, Baltimore, MD 21201

Telephone: 410-706-8292 Fax: 410-706-5017 E-mail: jpolli@rx.umaryland.edu

Number of text pages, tables, figures, references and words in abstract, introduction and discussion:

28 text pages

2 tables

10 figures

26 references

250 words in Abstract

749 words in Introduction

1267 words in Discussion.

List of Abbreviations:

hASBT, human apical sodium-dependent bile acid transporter; SLC, Solute carrier family; MDCK, Madin-Darby canine kidney; HBSS, Hanks balanced salt solution; ABL, aqueous boundary layer; UWL, unstirred water layer; QSAR, quantitative-structure activity relationship; NHS-SS-biotin, sulfosuccinimidyl-2-(biotinamido) ethyl-1,3-dithiopropionate; PBSCM, phosphate buffered saline with 0.1 mM $CaCl_2$ and 1 mM $MgCl_2$

Section Assignment:

Metabolism, Transport, and Pharmacogenomics

JPET Fast Forward. Published on October 12, 2006 as DOI: 10.1124/jpet.106.107433
This article has not been copyedited and formatted. The final version may differ from this version.

ABSTRACT

The objective was to investigate the interplay between transporter expression levels and substrate affinity in controlling the influence of aqueous boundary layer (ABL) resistance on transporter kinetics in an over-expression system. Taurocholate flux was measured across hASBT-MDCK monolayers on different occasions and kinetic parameters estimated with and without considering ABL. In error-free simulation/regression studies, flux values were generated across a range of J_{max}, K_t, and substrate concentrations. Similar evaluation was performed for transport inhibition studies. Additionally, simulation/regression studies were performed, incorporating 15% random error to estimate the probability of successfully estimating K_t. Across different occasions, experimental J_{max} and K_t estimates for taurocholate were strongly associated ($p<0.001$, $r^2=0.82$) when ABL was not considered. Simulation/regression results indicate that not considering ABL caused this association, such that K_t estimates were highly positively biased at high hASBT expression. In re-analyzing taurocholate flux data using the ABL-present model, K_t was relatively constant across occasions (about 5 μM) and not associated with J_{max} ($p=0.24$, $r^2=0.13$). Simulations suggest that J_{max} and K_t collectively determined ABL influence, which is most prominent under conditions of low monolayer resistance. Additionally, not considering ABL lead to negatively biased K_i estimates, especially at high J_{max}. Error-inclusive simulation/regression studies indicated that the probability of successfully estimating K_t depended on the contribution of ABL resistance to flux; when flux became increasingly ABL-limited, probability of success decreased. Results indicate that ABL resistance can bias K_t and K_i estimates from over-expression

systems, where the extent of bias is determined by transporter expression level and substrate affinity.

JPET Fast Forward. Published on October 12, 2006 as DOI: 10.1124/jpet.106.107433
This article has not been copyedited and formatted. The final version may differ from this version.

INTRODUCTION

Transfected cell models over-expressing specific transporters are a powerful tool to characterize substrate requirements of the transporter, including its ability to translocate drugs and prodrugs (Herrera-Ruiz et al., 2003; Tolle-Sander et al., 2004; Balakrishnan et al., 2005; Balakrishnan and Polli, 2006). Relative to native cells and *in vivo* systems, transfected cell models frequently have the advantage of characterizing a transporter without confounding variables, such as other simultaneously expressing transporters with overlapping substrate requirements. This benefit is achieved in part through high expression of the transporter of interest.

We recently developed a stably transfected cell model for the human apical sodium-dependent bile acid transporter (hASBT), using MDCK cells (Balakrishnan et al., 2005) that possesses several favorable properties, including high hASBT expression. This hASBT-MDCK model was further developed to yield kinetic estimates of substrates and/or inhibitors (e.g. J_{max}, K_t, K_i) that can be used for subsequent quantitative-structure activity relationship (QSAR) analysis. Thus, over-expression systems can be employed suitably for functional characterization of transporters.

In general, transporter expression level is expected to vary between occasions (i.e. vary between passages or cell culture conditions) (Yu et al., 1997; Polli et al., 2001). As an example in case, Figure 1 summarizes the kinetic analysis of hASBT-mediated taurocholate transport across hASBT-MDCK monolayers from twelve different occasions. As anticipated, J_{max} estimates varied several fold across occasions. K_t also varied across occasions and exhibited strong, positive association with J_{max} estimates ($p<0.0001$, $r^2=0.82$) (Fig. 1). Ideally, K_t can be expected to be constant across occasions and

independent of expression levels. However, J_{max} and K_t were estimated using a transport model that does not consider contribution of aqueous boundary layer (ABL) resistance. The present manuscript considers ABL as a lumped parameter composed of the apical unstirred water layer (UWL), support filter, and basolateral unstirred water layer (UWL). These diffusional barriers are encountered in flux studies across a monolayer grown on support filters. These diffusion barriers are lumped together, since it is difficult to reliably delineate them experimentally. Previous theoretical and experimental reports considered the presence of a single UWL situated apical to the biological membrane (i.e. an apical UWL) and indicated that failure to consider the UWL can result in inaccurate K_t estimates (Winne, 1973; Thomson and Dietschy, 1977; Winne, 1977; Winne, 1978; Thomson, 1979; Thomson and Dietschy, 1980; Barry and Diamond, 1984; Sinko et al., 1996). These reports have indicated the potential for UWL effects on active transport. Based on our previous data and reports by others, we hypothesized that high transporter expression can lower monolayer resistance, resulting in ABL-limited transport of solutes, leading to biased kinetic estimates if ABL is not considered.

One distinction between the present study and previous reports is the use of an over-expression system, where high expression level of transporter was achieved. Previous reports have clearly demonstrated UWL effect on K_t estimates, but it is not clear how variability in high transporter expression level impacts the quality of kinetic estimates, as observed in Fig. 1. Use of a monolayer flux assay also underpins a second difference between the present study and previous reports. Previous models assumed a single UWL, followed by a biological membrane (Winne, 1973; Thomson and Dietschy, 1977; Winne, 1977; Winne, 1978; Thomson, 1979; Thomson and Dietschy, 1980). These

studies evaluated *in vivo* perfusion studies, where the UWL represents a diffusion barrier between the bulk and the membrane. Unfortunately, the diffusion barriers in a monolayer flux configuration are less determinant since they are present at the apical interface, the basolateral interface, and via the support filter. The present study puts forth a transport model that reflects the cell culture monolayer flux assay. This transport model was extended to identify an inhibition model, an area unexplored by previous studies.

This study evaluates the interplay of transporter expression levels and substrate affinity in determining the role of ABL resistance on transporter kinetics using hASBT as a model transport system. The objectives were (1) to evaluate the effect of J_{max} on the contribution of ABL resistance to transporter kinetics, (2) to identify global kinetic conditions when ABL needs to be explicitly considered to accurately estimate kinetic parameters, and (3) to identify scenarios under which kinetic estimates are not reliable in spite of ABL consideration, due to ABL dominated transport kinetics. Objective 1 was carried out through a combination of empirical laboratory studies, as well as error-free simulation/regression studies. Objective 2 was conducted through error-free simulations of both transport and inhibition studies. Objective 3 was carried out through simulations incorporating 15% random error.

Given the broad utilization of over-expression systems to characterize transporter kinetics and given transporter expression variability over time, these results have implications in the development of high expression cell culture assays, as well as QSAR models and drug discovery efforts that rely on accurate kinetic parameter estimates.

JPET Fast Forward. Published on October 12, 2006 as DOI: 10.1124/jpet.106.107433
This article has not been copyedited and formatted. The final version may differ from this version.

METHODS

Transport Studies: ABL-absent Model. Figure 2 illustrates two competing models to describe bile acid transport across a hASBT-MDCK monolayer. The models differ in the absence or presence of an aqueous boundary layer (ABL). In panel A, the ABL-absent model is illustrated and only considers monolayer resistance to limit flux. Mechanisms of bile acid permeation across the monolayer are active hASBT transport and passive permeability. hASBT is located in the apical membrane and is the dominant mechanism for bile acid absorption (Dawson et al., 2003; Balakrishnan et al., 2005).

From Fig. 2 panel A, the ABL-absent model is

$$J = \frac{J_{\max} \cdot S}{K_t + S} + P_p \cdot S \qquad (1)$$

where J is bile acid flux when ABL is absent, J_{max} and K_t are the Michaelis-Menten constants for hASBT-mediated transport, S is bile acid substrate concentration, and P_p is the passive permeability coefficient. J_{max} and K_t are sometimes denoted Vmax and K_m, respectively, in the transporter literature.

Transport Studies: ABL-present Model. The ABL-present model is illustrated in Fig. 2 panel B. The term ABL includes the apical UWL, the support filter, and the basolateral UWL. ABL is considered a lumped parameter comprising these three components, since it is difficult to reliably delineate these individual barriers experimentally. The permeability across the ABL is P_{ABL}, such that this term represents the permeability across barriers other than the monolayer. As discussed below, P_{ABL} was estimated by measuring the permeability of taurocholate across blank filter in the absence of cells.

JPET Fast Forward. Published on October 12, 2006 as DOI: 10.1124/jpet.106.107433
This article has not been copyedited and formatted. The final version may differ from this version.

From Fig. 2 panel B, the apparent resistance to flux is

$$R_{app} = R_{ABL} + R_{mono} \quad (2)$$

where R_{app} is the apparent resistance, R_{ABL} is the resistance due to the ABL, and R_{mono} is the resistance due to the monolayer itself (i.e. monolayer resistance). Since permeability is the inverse of resistance,

$$\frac{1}{P_{app}} = \frac{1}{P_{ABL}} + \frac{1}{P_{mono}} \quad (3)$$

where P_{app} is the apparent permeability, P_{ABL} is the ABL permeability, and P_{mono} is the monolayer permeability. From the contributions of hASBT-mediated transport and parallel passive bile acid permeability to monolayer permeability,

$$P_{mono} = \frac{J_{\max}}{K_t + S} + P_p \quad (4)$$

Substituting eqn 4 into eqn 3,

$$\frac{1}{P_{app}} = \frac{1}{P_{ABL}} + \frac{1}{\frac{J_{\max}}{K_t + S} + P_p} \quad (5)$$

$$P_{app} = \frac{P_{ABL} \cdot \left(\frac{J_{\max}}{K_t + S} + P_p \right)}{P_{ABL} + \frac{J_{\max}}{K_t + S} + P_p} \quad (6)$$

Since $J_{ABL} = P_{app} \cdot S$,

$$J_{ABL} = \frac{P_{ABL} \cdot \left(\frac{J_{\max}}{K_t + S} + P_p \right) \cdot S}{P_{ABL} + \frac{J_{\max}}{K_t + S} + P_p} \quad (7)$$

JPET Fast Forward. Published on October 12, 2006 as DOI: 10.1124/jpet.106.107433
This article has not been copyedited and formatted. The final version may differ from this version.

where J_{ABL} is bile acid flux when ABL is present. Equation 7 is denoted the ABL-present model.

Comparison of the ABL-present Model to the Uptake Model of Winne. Equation 7 differs from the uptake model of Winne (Winne, 1977), which can be written as

$$J_{UWL} = P_{UWL}\left\{S + \frac{q}{2}\left(\frac{K_t}{q} + \frac{J_{\max}}{P_{UWL}} - S\right) - \sqrt{\frac{q^2}{4}\left(\frac{K_t}{q} + \frac{J_{\max}}{P_{UWL}} - S\right)^2 + qK_tS}\right\} \quad (8)$$

where J_{UWL} is the flux when a single UWL is present prior to the membrane, P_{UWL} is the permeability of the UWL, and $q = \frac{P_{UWL}}{P_p + P_{UWL}}$. J_{max}, K_t, P_p, and S represent the same parameters in both eqn 7 and 8. Equation 8 simplifies the original Winne equation by equating the area of the UWL to the area of the membrane, as well as by substituting P_{UWL} for the ratio of the diffusivity coefficient to the UWL thickness.

Underpinning the difference between the ABL-present model and the Winne uptake model is the number and arrangement of diffusion barriers, relative to the biological membrane. In the uptake model of Winne, only an apical UWL is present. Winne et al. applied eqn 8 to assess the role of the UWL in the absorption of phenylalanine (Winne et al., 1979) using the perfused rat jejunal loop. Justification of Winne's model would appear to be the presence of an UWL within the loop lumen, with no other significant diffusion barriers, except the jejunal loop membrane. Strength of the Winne uptake model is its differentiation between the bulk donor solution concentration (S) and the concentration at the UWL-membrane interface, particularly compared against the ABL-present model.

Winne's model cannot be applied to transport studies across a cell monolayer since it fails to consider diffusional resistances other than the apical UWL. Complicating this scenario is the arrangement of a diffusion barrier on the luminal side of the monolayer (i.e. apical UWL) and two diffusion barriers on the other side (i.e. support filter and basolateral UWL). A further limitation is an insufficient understanding of these diffusion barriers since the permeability of each barrier is difficult to measure in a reliable manner. The approach in the present manuscript was to characterize these three barriers as a single resistivity R_{ABL}, per eqn 2 (i.e. a single permeability P_{ABL}, per eqn 3). This single barrier is denoted the aqueous boundary layer (ABL). P_{ABL} was estimated by measuring the permeability of taurocholate across blank filter in the absence of cells (Yu and Sinko, 1997). Briefly, in Fig 2 panel B, when monolayer present, the support filter, the apical unstirred water layer, and the basolateral unstirred water layer are present and collectively denoted as the ABL. When monolayer absent, these elements are still present. Hence, ABL was estimated by measuring taurocholate flux across blank support filter.

Measure of Monolayer Resistance. Equation 1 and 7 (i.e. the ABL-absent and ABL-present models) each allow for a non-linear, Michaelis-Menten type component, as well as linear, passive transport component. The two models differ with respect to the contribution of the ABL on flux. In Fig. 2 panel A, ABL is absent, such that the only rate-limiting barrier in eqn 1 is the monolayer. In Fig. 2 panel B, ABL is present, reflecting that ABL contributes as a barrier to flux in eqn 7. Qualitatively, a high ABL resistance relative to monolayer resistance results in flux limited by ABL. On the other

JPET Fast Forward. Published on October 12, 2006 as DOI: 10.1124/jpet.106.107433
This article has not been copyedited and formatted. The final version may differ from this version.

hand, high monolayer resistance relative to ABL results in flux limited by monolayer, as in Fig. 2 panel A.

The ratio of flux from the ABL-present model to the flux from the ABL-absent model (J_{ABL}/J) is used to assess the impact of ABL on flux. Of note, J_{ABL}/J is also numerically equivalent to the fraction of total flux resistance that is attributed to the monolayer:

$$F_{mono} = \frac{J_{ABL}}{J} \qquad (9)$$

where F_{mono} is the fraction of total flux resistance that is due to the monolayer. Appendix 1 derives eqn 9. Monolayer resistance excludes components of the ABL such as the support filter and apical and basolateral UWLs. From eqn 9, J_{ABL}/J = 1 indicates that flux is limited by monolayer resistance only (i.e. F_{mono} = 1). Meanwhile, J_{ABL}/J = 0.1 indicates that the monolayer contributes to only 10% of the total resistance (i.e. F_{mono} = 0.1), with the ABL contributing the remaining 90%.

Transport Inhibition Studies. For competitive inhibition studies of taurocholate transport by bile acids, the following transport inhibition model describes taurocholate transport when ABL is absent:

$$J = \frac{J_{\max} \cdot S}{K_t\left(1 + I/K_i\right) + S} + P_p \cdot S \qquad (10)$$

where I is the concentration of inhibitor (i.e. inhibitory bile acid) and K_i is inhibition constant. S is substrate concentration (i.e. taurocholate concentration); J_{max}, K_t, and P_p

JPET Fast Forward. Published on October 12, 2006 as DOI: 10.1124/jpet.106.107433
This article has not been copyedited and formatted. The final version may differ from this version.

characterize substrate transport parameters. Eqn 10 is denoted the ABL-absent inhibition model.

When the ABL is included, the competitive inhibition model becomes:

$$J_{ABL} = \frac{P_{ABL} \cdot \left(\frac{J_{max}}{K_t\left(1 + I/K_i\right) + S} + P_p \right) \cdot S}{P_{ABL} + \left(\frac{J_{max}}{K_t\left(1 + I/K_i\right) + S} \right) + P_p} \qquad (11)$$

where P_{ABL} is ABL permeability. Eqn 11 is denoted the ABL-present inhibition model. This model is derived in Appendix 2.

Taurocholate Transport across hASBT Monolayers. Taurocholate was used as a model substrate for hASBT. On twelve occasions, apical-to-basal taurocholate flux was measured across an hASBT-MDCK monolayer model, as described previously(Balakrishnan et al., 2005). Briefly, hASBT-MDCK cells were seeded at a density of 0.75 million cells/cm^2 on support filter (Corning; Corning, NY; polyester Transwell, 0.4μ pore size, 1cm^2). Kinetics of hASBT-mediated taurocholate flux was assessed from transport studies (n = 3) at differing donor concentrations (1-200 μM spiked with [^{3}H]-taurocholate). Transport was performed using HBSS with 10mM HEPES (pH 6.8) at 37^{o}C and 50 rpm. Sample was obtained from basolateral compartment at 30 min, well after steady-state was attained (by 5 min). Sink-conditions prevailed in all studies. Sink conditions refer to the low accumulation of substrate into basolateral compartment, as to essentially not bias results. This situation was attained by

assuring that substrate concentration in the receiver compartment never exceeded 10% of donor substrate concentration. In all studies, [^{14}C]-mannitol was used to monitor monolayer integrity. In all cases, mannitol permeability was less than 4.0×10^{-6} cm/sec. Mass balance ranged from 90 to 120%.

Flux data from each occasion was fitted to the ABL-absent model (i.e. eqn 1) as well as the ABL-present model (i.e. eqn 7), providing estimates for J_{max}, K_t, and P_p for each of the two model scenarios. In eqn 7, P_{ABL} was assigned, based upon taurocholate flux data across support filters without monolayers, as discussed below.

Non-linear regression to eqn 1 and 7 was performed using SigmaPlot2000 (SPSS Inc.; Chicago, IL). Correlation amongst parameter estimates was evaluated using Pearson correlation coefficient using SPSS 12.0 (SPSS Inc.; Chicago, IL).

Taurocholate Uptake into hASBT Monolayers. In contrast to transport studies, uptake studies only concern the translocation of taurocholate across the apical membrane and into the cytosol. On five occasions, taurocholate uptake into hASBT-MDCK monolayers were assessed as described previously (Balakrishnan et al., 2005).

Briefly, hASBT-MDCK cells were seeded at a density of 1.5 million cells/well on 12 well plates (Corning; Corning, NY). Kinetics of hASBT-mediated taurocholate uptake was assessed from uptake studies (n = 3) at differing donor concentrations (1-200 μM spiked with [^{3}H]-taurocholate). Studies were performed using HBSS with 10mM HEPES (pH 6.8) at 37^{o}C and 50 rpm for 10 min. The 10 min time point was selected since taurocholate uptake was linear over 10 min (Balakrishnan et al., 2005). The donor solution was removed and the cells were washed three times with chilled sodium free

buffer. Cells were lysed using 0.25 ml of 1 N NaOH and neutralized with 0.25 ml of 1 N HCl. Cell lysate was then counted for associated radioactivity using a liquid scintillation counter (Beckman Instruments; Fullerton, CA).

Flux data from each occasion were fitted to the ABL-absent model (i.e. eqn 1) as well as the ABL-present model (i.e. eqn 7), providing estimates for J_{max}, K_t, and P_p for each of the two model scenarios. In eqn 7, P_{ABL} was assigned, based upon diazepam uptake data, as discussed below. Non-linear regression to eqn 1 and 7 was performed using SigmaPlot2000 (SPSS Inc.; Chicago, IL). Correlation amongst parameter estimates was evaluated using Pearson correlation coefficient using SPSS 12.0 (SPSS Inc.; Chicago, IL).

Taurocholate Transport across Support Filter without hASBT-MDCK Monolayer to Estimate P_{ABL} for Transport Studies. It is difficult to directly measure the net effect of the aqueous boundary layer at the apical interface, the aqueous boundary layer at the basolateral interface, and the plastic filter (i.e. P_{ABL}) when cell monolayer is present. When an estimate of P_{ABL} is sought, a common approach to measure P_{ABL} is to employ blank filter (Imanidis et al., 1996; Yu and Sinko, 1997). Hence, taurocholate transport across blank support filters (i.e. polyester Transwell without cell monolayer) was performed as described above. The underlying assumption in this approach is that the ABL in the ABL-present model in Fig. 2 panel B is the same whether a monolayer is present or not present. Flux studies were performed using HBSS with 10mM HEPES (pH 6.8) at 37^{o}C and 50 rpm. At 5 min, sample was collected from the receiver compartment and allowed for sink conditions to be maintained. Taurocholate

JPET Fast Forward. Published on October 12, 2006 as DOI: 10.1124/jpet.106.107433
This article has not been copyedited and formatted. The final version may differ from this version.

permeability across blank support filters was 66.1(±6.0) x 10^{-6} cm/sec, which was taken to be equal to P_{ABL}. This value was in agreement with that of (Buur and Mork, 1992).

P_{ABL} served as a lumped parameter in eqn 7 and 11 to characterize ABL, since it is difficult to reliably measure the permeability of the apical unstirred water layer, the support filter, and the basolateral unstirred water layer individually. It should be noted that Yu and Sinko (Yu and Sinko, 1997) and Adson et al. (Adson et al., 1994) have attempted to uncouple some of these barrier components, although active transport was not considered. Adson et al. (Adson et al., 1994) calculated a value for the permeability of the support filter, based upon a porous membrane model and parameters provided by the manufacturer, an approach that may be unreliable (Yu and Sinko, 1997). Yu and Sinko (Yu and Sinko, 1997) employed an empiric model to simultaneously estimate support filter permeability and the UWLs; the approach required "labor-intensive" flux studies across blank filters, where hydrodynamics was varied (Yu and Sinko, 1997).

Diazepam Uptake into hASBT-MDCK Monolayer to Estimate P_{ABL} for Uptake Studies. Uptake of radiolabeled diazepam into hASBT-MDCK cells was assessed to estimate P_{ABL} for uptake studies. By virtue of its high permeability across bilayers, diazepam is a commonly used marker for measurement of UWL resistance. After 30 sec, uptake was stopped by freezing the cells instantaneously over dry ice in alcohol. This process rigidized cell membrane and aimed to minimize back diffusion. Cells were washed twice with ice cold buffer and lysed using 1%Triton in 1 N NaOH. Diazepam in cell lysate was quantified using a scintillation counter. Diazepam permeability was 150(±3) x 10^{-6} cm/sec, which was taken to be equal to P_{ABL} for uptake studies. This P_{ABL}

value from the uptake configuration is greater than P_{ABL} from the transport configuration, presumably reflecting that only the apical UWL is present in case of uptake configuration, while basolateral UWL and filter support are additional diffusion barriers in the transport configuration.

Simulations for Objective 1: Impact of Varying J_{max} on ABL Contribution. The ABL-present model for transport (i.e. eqn 7) was used to simulate flux data. No error was incorporated into these simulations. Values for K_t, P_p, and P_{ABL} were 5 μM, $0.5x10^{-6}$ cm/sec, and $70x10^{-6}$ cm/sec, respectively. These values were selected based upon experimental measurements of K_t, P_p, and P_{ABL}. Values for substrate concentration and J_{max} ranged from 0.5 to 1000 μM and 0.00001 to 0.01 nmoles/cm^2/sec, respectively. J_{max} values were selected based upon observed J_{max} values. Error-free simulations were systematically performed for all combinations of parameter values. Error-free flux data were similarly simulated using the ABL-absent model (eqn 1).

Simulated J_{ABL} data were subsequently regressed on to the ABL-absent model to yield estimates of K_t, J_{max}, and P_p. This approach quantified bias in K_t, J_{max}, and P_p parameter estimates when ABL was ignored.

Simulations for Objective 2: Identification of Global Kinetic Conditions that Require ABL Consideration. Simulations were performed to identify global kinetic conditions when ABL needs to be explicitly considered to accurately estimate kinetic parameters (e.g. K_t, J_{max}, or K_i). Simulations were performed for transport and transport inhibition studies.

Transport data were simulated under both ABL-present and ABL-absent scenarios. P_p and P_{ABL} were fixed to be $0.5x10^{-6}$ cm/sec and $70x10^{-6}$ cm/sec, respectively. Values for K_t and J_{max} ranged from 0.1 to 10,000 μM and 0.00003 to 0.01 nmoles/cm^2/sec, respectively. Substrate concentration was fixed to one-tenth K_t value for each simulation. The impact of ABL was assessed by the ratio J_{ABL}/J. J_{ABL}/J greater than 0.9 indicated that ABL contribution is not significant. J_{ABL}/J less than 0.9 indicated that ABL is significant, such that ABL needs to be considered to accurately estimate kinetic parameters.

Inhibition data were simulated using the ABL-absent and ABL-present models in a similar fashion (i.e. eqn 10 and 11). Substrate concentration, K_t, and K_i values were 2.5 μM, 5 μM and 50 μM, respectively. Inhibitor concentration ranged from 0.1 to 1,000 μM. J_{max} ranged from 0.00001 to 0.01 nmoles/cm^2/sec. Simulated J_{ABL} was subsequently regressed on to the ABL-absent inhibition model to yield estimates of K_i. K_t, J_{max}, and P_p were assigned to the values used in generating the simulated data. This approach quantified bias in K_i parameter estimates when ABL was ignored.

Simulations For Objective 3: Identification of Global Kinetic Conditions when K_t Estimates are Unreliable as a Result of ABL Contribution. Equation 7 was employed using $P_p=0.5x10^{-6}$ cm/sec and $P_{ABL}=70x10^{-6}$ cm/sec to generate initial error-free flux data. Fifteen scenarios were systematically evaluated for five levels of K_t (1, 3, 5, 10, and 25 μM) at each of three levels of J_{max} (0.0001, 0.0003, and 0.001 nmol/s/cm^2). Substrate concentrations were 1/20, 1/10, 1/5, 1/2, 1, 2, 5, 10, and 20-fold of true K_t value. For the scenario K_t = 1 μM and J_{max} = 0.001 nmol/s/cm^2, substrate concentrations 40, 80, and160

μM were also included. Flux data for every substrate concentration were simulated in triplicate for each occasion, mimicking triplicate design of *in vitro* laboratory studies. Random error reflecting %CV = 15% was incorporated into simulated flux data. For each of these 15 scenarios, simulations were performed on 100 occasions. Data from each occasion were regressed onto eqn 7 to estimate K_t, J_{max}, and P_p, with emphasis on K_t. For each simulation scenario, K_t estimates from each of the 100 occasions was used to calculate the probability of calculating meaningful K_t estimates (i.e. statistically differed from zero based upon 95% confidence interval). Non-linear regression to eqn 7 was performed using WinNonlin Professional ver 4.1 (Pharsight Corp., ver. 4.1; Mountainview, CA), which was kindly donated by Pharsight Corp.

Cell Surface Biotinylation and Immunoblotting. Figure 1 provided motivation for the present study, presuming that variation in J_{max} was ascribed to variation in hASBT expression. The rank-order agreement between cell surface hASBT expression level and J_{max} was assessed though parallel studies involving Western blots and taurocholate transport studies.

hASBT-MDCK monolayers were grown as described above (Balakrishnan et al., 2005) and treated with varying levels of sodium butyrate to modulate hASBT expression level. hASBT-MDCK monolayers were treated with either 10 mM, 5 mM, or no sodium butyrate, to yield monolayers corresponding to three levels of hASBT expression (i.e. high, intermediate, and low). Additionally, untransfected MDCK monolayers were also treated with 10 mM sodium butyrate as negative control

Cell surface expression of hASBT was determined by treating cells with the membrane-impermeant biotinylation reagent NHS-SS-biotin (Pierce Chemical Co.; Rockford, IL) for 30 min at room temperature (Visiers et al., 2003). After several washes in PBSCM, cells were disrupted in Lysis buffer [25 mM Tris HCl (pH 7.5), 300 mM NaCl, 1 mM $CaCl_2$, 1% Triton X-100, and 0.5% Sigma Protease Inhibitor Cocktail] for 30 min at 4 °C. Biotinylated proteins were recovered by overnight incubation with 100 µL of streptavidin-agarose beads per sample (Pierce Chemical Co.; Rockford, IL) at 4 °C using end-over-end rotation. The following day, the beads were washed once with Lysis buffer, once in High-Salt lysis buffer (same as Lysis buffer except with 500 mM NaCl and 0.1% Triton X-100), and finally twice with 50 mM Tris (pH 7.5). Biotinylated proteins were eluted using 100 µL of SDS-PAGE Laemelli buffer (pH 6.8; Sigma Aldrich; St. Louis, MO) for 10 min at 85 °C. For each sample, 20 µL was applied to a 12.5 % SDS-PAGE gel (BioRad; Hercules, CA) and transferred to a PVDF membrane for immunoblotting. Since hASBT was constructed with a V5 epitope (Balakrishnan et al., 2005), hASBT was detected with the anti-V5/horse radish peroxidase-conjugated antibody (1:1000 dilution; Invitrogen Corp, Carlsbad, CA) directed to the V5 epitope located at the C-terminus. Bands were detected by chemiluminesence using ECL plus Western Blotting Detection System (Amersham Biosciences; Buckinghamshire, UK). Blots were then stripped via ECL Detection System protocols and reprobed for the presence of the constitutively expressed plasma membrane marker α-integrin, using anti-integrin α2/VLA-2α antibody, followed by donkey anti-mouse HRP-conjugated secondary antibody. α-integrin represents a positive control for cell surface biotinylation of plasma membrane proteins. In order to confirm cell membrane integrity during

biotinylation, the same membrane was also probed for the absence of calnexin, a 90 kDa housekeeping protein present in whole cell lysate preparations, using anti-calnexin antibody and donkey anti-rabbit HRP-conjugated secondary antibody. Calnexin was absent from biotinylated samples (data not shown), ensuring that only cell surface proteins were biotin-labeled and immunoblotted.

Densitometry measurements of hASBT expression level were not performed, since densitometry unfortunately requires high protein expression and α-integrin was not sufficiently high for densitometric measurement. Rather, post-hoc analysis of band density using pixel intensity was assessed using NIH Image software (v. 1.6.3) for each sodium butyrate treatment level (as well as control untransfected MDCK monolayers). Using a standard rectangular box in NIH Image, pixel intensity of hASBT was measured and normalized against pixel intensity of α-integrin; pixel intensity ratio of hASBT versus α-integrin from each treatment was corrected for background control via subtraction of pixel intensity ratio from untransfected MDCK monolayers and interpreted as hASBT expression level (relative to integrin).

Taurocholate flux in the presence and absence of sodium was measured as described above. J_{max} was estimated and compared to Western blot analysis. Results are shown in Appendix 3.

RESULTS

Simulations for Objective 1: Impact of Varying J_{max} on ABL Contribution. Taurocholate permeability across blank support filters was 66.1(±6.0) x 10^{-6} cm/sec. Hence, P_{ABL} was fixed at $70x10^{-6}$ cm/sec in all simulations.

Figure 3 is a contour plot of the ratio of J_{ABL} versus J, as a function of J_{max} and substrate concentration. J_{ABL}/J greater than 0.9 indicates that ABL contribution was not significant. J_{ABL}/J less than 0.9 indicates that ABL contribution is significant. At a very low J_{max} of 0.00003 nmoles/cm^2/sec, J_{ABL}/J always exceeded 0.9, regardless of substrate concentration. For higher J_{max} scenarios, J_{ABL}/J dropped below 0.9 at low substrate concentrations, but generally returned to about unity at high substrate concentration. At very high J_{max} of 0.01 nmoles/cm^2/sec, flux from the ABL-present models was 20-fold lower than flux from the ABL-absent model at low substrate concentration (i.e. J_{ABL}/J about 0.05). These simulations indicate that ABL limits flux significantly at high J_{max} and low substrate concentration. These simulations follow the results observed in earlier studies (Thomson and Dietschy, 1977; Thomson and Dietschy, 1980), although the present manuscript attempts to highlight the influence of J_{max} (i.e. expression level), since expression level of transporters can vary across occasions in a cell culture system.

From eqn 3, J_{ABL}/J in Fig. 3 can also be interpreted to be the fraction of total flux resistance that is attributed to the monolayer, F_{mono}. Under conditions of high J_{max} and low substrate concentration, F_{mono} is low, such that ABL is dominant. At low J_{max} and/or high substrate concentration, F_{mono} is large, such that monolayer resistance is dominant and ABL effect is not significant.

Simulated flux data from the ABL-present model were regressed onto the ABL-absent model to yield estimates of K_t and J_{max}, as well as Pp. This approach quantified

JPET Fast Forward. Published on October 12, 2006 as DOI: 10.1124/jpet.106.107433
This article has not been copyedited and formatted. The final version may differ from this version.

bias in K_t and J_{max} parameter estimates when ABL is ignored. Parameter value ranges reflect the range of values observed experimentally. Figure 4 plots the true and fitted estimates for K_t as a function of J_{max}. The true K_t (i.e. the K_t value employed in simulations) was 5 μM. In Fig. 4, the estimated K_t value was about the same as the true K_t value when J_{max} was very low. K_t estimates below J_{max} of 0.00003 nmole/cm^2/sec reflected low bias of 0 to 5%. For J_{max} of 0.0003 nmole/cm^2/sec, K_t estimate was about 2-fold higher than true K_t. For progressively higher J_{max}, K_t estimates exhibited very high positive bias (almost 1000-fold larger). These results indicate that failure to consider ABL can lead to erroneously large K_t estimates at high J_{max}. These results are consistent with experimental taurocholate data in Fig. 1, where high K_t was associated with high J_{max}. Simulation results suggest that, in Fig. 1, K_t estimates were over-estimated due to low monolayer resistance (i.e. low F_{mono}), particularly on occasions when J_{max} was high.

Unlike ABL effect on K_t estimates, ABL had no impact on J_{max} estimates (data not shown). This lack of effect is in agreement with earlier studies (Thomson and Dietschy, 1980). There was practical identity between fitted J_{max} and true J_{max} values, indicating that the use of the ABL-absent model did not bias J_{max} estimates. ABL only impacted K_t estimates and not J_{max}. Interesting, the ABL-absent and ABL-present models provided equally good fits to simulated data, based on AIC and r^2 (data not shown).

In the light of above observations, Fig. 5 re-evaluates experimental taurocholate data. The ABL-present model was employed to obtain K_t and J_{max} estimates, whose values are plotted in Fig. 5. J_{max} ranged between 0.0001 to 0.001 nmole/sec/cm^2. K_t ranged from about 1 to 12 μM with an average K_t estimate of approximately 5 μM. Compared to regression results from the ABL-absent model (i.e. Fig. 1), estimates of K_t

JPET Fast Forward. Published on October 12, 2006 as DOI: 10.1124/jpet.106.107433
This article has not been copyedited and formatted. The final version may differ from this version.

were about 2-fold to 3-fold lower from the ABL-present model. J_{max} estimates were the same from each model from both models, as expected from above simulation results. Additionally, Pp estimates were the same from both models (data not shown). In contrast to Fig. 1, there was no association between K_t estimates and J_{max} estimates in Fig. 5 ($p = 0.24$; $r^2 = 0.13$). This lack of association indicates that correcting for ABL influence lead to a more accurate and less biased estimate of K_t.

UWL effects in taurocholate uptake data were also corrected in an analogous fashion (see Appendix 4). It should be noted that the K_t estimates for uptake and transport studies were similar (both about 5 μM), indicating that the configuration of the assay (i.e. uptake versus transport) did not affect K_t estimate. This result supports the apical membrane serving as the rate-limiting barrier within the monolayer in transport studies. Hence, a basolateral transporter such as Ostα-Ostβ is not contributing as the rate-limiting barrier. Ostα-Ostβ is a heteromeric transporter that has been recently identified to translocate bile acids in the enterocyte basolateral membrane (Ballatori et al., 2005; Dawson et al., 2005).

Simulations for Objective 2: Identification of Global Kinetic Conditions that Require ABL Consideration. Since high J_{max} can lead to ABL-limited transport and subsequent positive bias in K_t estimate, a second objective was to identify global kinetic conditions when ABL needs to be explicitly considered to accurately estimate kinetic parameters. This assessment was carried out via simulations of the ABL-absent and ABL-present models, using parameter values that reflect the range of observed

JPET Fast Forward. Published on October 12, 2006 as DOI: 10.1124/jpet.106.107433
This article has not been copyedited and formatted. The final version may differ from this version.

parameters. The impact of ABL was assessed by J_{ABL}/J; J_{ABL}/J less than 0.9 indicated that ABL is significant.

Figure 6 plots J_{ABL}/J as a function of K_t at varying J_{max} and illustrates the interplay of J_{max} and K_t in determining ABL impact. In Fig. 6, at low J_{max} and high K_t (i.e. poor substrate for transporter), ABL is not significant, as observed by J_{ABL}/J greater than 0.9 (i.e. $F_{mono} > 0.9$). Overall flux is controlled by monolayer resistance and not by ABL. Meanwhile, for large J_{max} and/or low K_t, J_{ABL}/J is low, which reflects a significant role of ABL. In the case of both high J_{max} and low K_t, J_{ABL}/J (i.e. F_{mono}) is less that 0.1, reflecting ABL accounts for over 90% of total resistance to transport. Figure 6 is consistent with observed taurocholate data plotted in Fig. 1 and 5, where ABL was modestly important for low J_{max} and very important at high J_{max}. Similar dependence on J_{max} is evident in Fig. 6.

These results comparing J_{ABL} and J indicate that ABL needs to be explicitly considered for all potent substrates (i.e. K_t less than or equal to 10 μM), even in low expression systems (i.e. $J_{max} > 0.00003$ nmole/cm^2/sec). Additionally, at J_{max} greater than 0.001 nmole/cm^2/sec, as observed for hASBT-MDCK, ABL needs to be considered even when Kt is as large as 100 μM. Given the high hASBT expression from the current hASBT-MDCK model, the simulations anticipate the need to employ the ABL-present model for all native bile acids. Interestingly, these simulations suggest lowered hASBT expression (i.e. lower J_{max}) as an approach to minimize ABL influence on transport. Future laboratory studies will employ hASBT-MDCK monolayers with reduced hASBT expression, especially for potent substrates, in order to minimize ABL influence.

Simulation studies were also performed for transport inhibition studies, to identify global kinetic conditions that require ABL consideration for accurate K_i estimation. Previous studies have not examined diffusion barrier effects on K_i estimation. Figure 7 plots J_{ABL}/J as a function of inhibitor concentration and J_{max}. At low J_{max}, J_{ABL}/J was greater than 0.9, indicating lack of ABL effect. However, J_{ABL}/J decreased with increasing J_{max} and reached 0.4 and lower at J_{max} = 0.01 nmole/cm^2/sec, indicating significant ABL effect under these conditions. These observations are similar to the results from the corresponding transport simulations (Fig. 3). The consequence of low J_{ABL}/J (observed in Fig. 7) on K_i estimates is shown in Fig. 8. Figure 8 plots the true and fitted estimates for K_i as a function of J_{max}. The true K_i (i.e. the K_i value employed in simulations) was 50 μM. For J_{max} of 0.0001 nmole/cm^2/sec, K_i estimate was about 27 μM (i.e. about 2-fold lower than true K_i). For progressively higher J_{max}, K_i estimates exhibited very high negative bias (about 10-fold lower). These results indicate that failure to consider the contribution of ABL leads to erroneously low K_i estimates, particularly at high J_{max}. Figure 9 further details the interplay of J_{max} and K_t in determining the impact of ABL on bias in K_i estimates, using error-free data. In all situations, K_i estimates were negatively biased, particularly for low K_t values, regardless of J_{max}. Bias is greatest at low K_t values and high J_{max}, due to low monolayer resistance for the substrate. In essence, when ABL is not considered, K_i "takes credit" for the ABL effect, leading to biased K_i estimate. This analysis of simulation/regression indicates that bias in K_i estimates is greatest when the substrate is very potent (i.e. low K_t), and this effect is amplified at high J_{max}.

These simulation results are consistent with experimental taurocholate self-inhibition data (Table 1). For each of the twelve occasions, the ABL absent inhibition model (Eq. 10) provided a lower K_i than did the ABL present inhibition model (Eq. 11).

Simulations for Objective 3: Identification of Global Kinetic Conditions when K_t Estimates are Unreliable as a Result of ABL Contribution. Figure 6 indicates that J_{ABL} is less than 10% of J for several scenarios. These observations from error-free simulations motivated a more detailed evaluation, using simulations that incorporate 15% random error. This evaluation aimed to identify conditions under which kinetic parameters cannot be precisely estimated due to the combination of ABL-controlled transport and modest experimental variability.

Table 2 indicates the probability of successfully estimating K_t estimates under different scenarios of K_t and J_{max} using error-inclusive simulated flux data. Estimation of K_t was deemed successful if the 95% confidence interval for the K_t estimate did not include zero. For each of the fifteen scenarios, Table 2 also denotes the percent of total resistance that is attributed to ABL. As expected from objective 2 results, the probability of successful K_t estimation was low when J_{max} was high and true K_t was less than 10 μM. For example, the probability was only 10% when true K_t = 1 μM and J_{max} = 0.001 nmoles/cm^2/sec. In general, the probability of success increased for progressively lower J_{max} and progressively higher K_t. For example, when true Kt = 5 μM and J_{max} = 0.0001 nmoles/cm^2/sec, the probability was 91%. This trend is attributed to progressively lower contribution of ABL to overall control of flux. To a first approximation, the probability of failing to estimate K_t is equal to the percent resistance due to ABL. J_{max} was

successfully estimated in almost all occasions, as expected based on previous studies (Thomson and Dietschy, 1980) and results from objective 2 in the present study.

A result not anticipated from error-free simulation is the modest decrease in successful K_t estimation in Table 2 at high K_t. At K_t of 25 μM, the above trend was reversed, such that probability of success drops for progressively lower J_{max}. At high K_t scenarios, the passive flux component contributes significantly to overall flux, especially when J_{max} is low, leading to modest decrease in successful K_t estimation.

DISCUSSION

Kinetics of hASBT-Mediated Taurocholate Flux using ABL-Absent Model. hASBT is under investigation as a target to increase the oral absorption of drug candidates through a prodrug approach (Balakrishnan and Polli, 2006). An hASBT-MDCK monolayer model was previously developed (Balakrishnan et al., 2005). Specificity of hASBT-mediated transport of taurocholate was based upon a number of observations (e.g. hASBT-transfected versus mock-transfected studies, no-sodium versus sodium-containing studies, apical-to-basolateral versus basolateral-to-apical studies, lack of taurocholate inhibition by DIDS or probenecid, confocal imaging of hASBT in the hASBT-MDCK model, and similar Kt estimates in monolayer transport and uptake studies). It should be noted that while the hASBT-MDCK is employed to elucidate the substrate requirements of hASBT, bile acids are substrates for the recently identified Ostα-Ostβ heteromeric transporter in the enterocyte basolateral membrane (Ballatori et al., 2005; Dawson et al., 2005). However, as noted above, results here do not reflect

Ostα-Ostβ kinetic activity, but reflect hASBT kinetic activity, since K_t estimates for uptake and transport studies were similar. Additionally, taurocholate transport was unaffected by the Ostα-Ostβ inhibitor bromosulphaelin (BSP) (Seward et al., 2003; Balakrishnan et al., 2006) .

Taurocholate flux across hASBT-MDCK monolayers are routinely performed. Motivation for the present study was the observed positive association between taurocholate J_{max} and K_t estimates, where the ABL-absent model was used. The ABL-absent model is the model typically used in analyzing flux data from cell culture transporter assay systems. K_t and J_{max} estimates exhibited significant variation across occasions. K_t ranged from about 2 to 27 μM. J_{max} ranged between 0.0001 to 0.001 nmole/sec/cm^2. In Fig. 1, there was a strong linear association between K_t and J_{max} estimates (r^2 = 0.82; $p > 0.001$). Variability in J_{max} can be ascribed to variability in hASBT expression (see Appendix 3). However, variability in K_t, particularly K_t variation that is associated with J_{max}, was difficult to explain. This association yielded the following hypothesis: high transporter expression can lower monolayer resistance, resulting in ABL-limited transport of solutes, leading to biased kinetic estimates if ABL is not considered. Three objectives were pursued in challenging this hypothesis.

Simulations for Objective 1: Impact of Varying J_{max} on ABL Contribution. The first objective was to evaluate the effect of J_{max} on the contribution of ABL resistance to transporter kinetics. Objective 1 was carried out through a combination of empirical laboratory studies, as well as error-free simulation/regression studies. Results indicate that failure to consider ABL can lead to erroneously large K_t estimates at high J_{max}.

Results were consistent with experimental taurocholate data in Fig. 1, where high K_t was associated with high J_{max}. Simulation results suggest that, in Fig. 1, K_t estimates were over-estimated due to low monolayer resistance (i.e. low F_{mono}), particularly on occasions when J_{max} was high.

Fig. 5 re-evaluates experimental taurocholate data. The ABL-present model was employed to obtain K_t and J_{max} estimates, whose values are plotted in Fig. 5. Compared to regression results from the ABL-absent model (i.e. Fig. 1), estimates of K_t were about 2-fold to 3-fold lower from the ABL-present model. In contrast to Fig. 1, there was no association between K_t estimates and J_{max} estimates in Fig. 5 ($p = 0.24$; $r^2 = 0.13$). This lack of association indicates that correcting for ABL influence lead to a more accurate and less biased estimate of K_t. It should be noted that variability in K_t was not completely eliminated. Contributions to the remaining unexplained variation are variation in flux measurements and parameter estimation error.

Simulations for Objective 2: Identification of Global Kinetic Conditions that Require ABL Consideration. The second objective was to identify global kinetic conditions when ABL needs to be explicitly considered to accurately estimate kinetic parameters. Objective 2 was conducted through error-free simulations of both transport and inhibition studies. Results indicate that ABL can generally modulate hASBT kinetics, particularly for all potent substrates, even in low expression systems. Additionally, at J_{max} greater than 0.001 nmole/cm^2/sec, as observed for hASBT-MDCK, ABL needs to be considered even when K_t is as large as 100 μM. Interestingly, results suggest lower hASBT expression as an approach to minimize ABL influence on transport. Simulation

studies were also performed for transport inhibition studies, which revealed that failure to consider the contribution of ABL leads to erroneously low K_i estimates, particularly at high J_{max}.

However, it should also be noted that ABL effect depends on substrate K_t and J_{max} in the particular assay system, and therefore ABL is not always significant. For example, ABL influence is not significant for a low affinity transporters like hPEPT1. Herrera-Ruiz et al. developed a stably transfected hPEPT1-MDCK cell line with varying expression levels (Herrera-Ruiz et al., 2003). K_t of glycyl sarcosine was 400 μM. From Fig. 6 here, it can be inferred that ABL influence would not be significant for this substrate until very high J_{max} (i.e. until over 0.001 nmoles/sec/cm^2) is attained. Lack of effect was evident experimentally from Herrera-Ruiz et al., since glycyl sarcosine K_t estimate did not vary with varying J_{max} (Herrera-Ruiz et al., 2003). A second example illustrates a modest ABL effect in an organic anion transporter 3 (OAT3) study (Zhang et al., 2004). Uptake of estrone sulfate into rabbit OAT3-CHO exhibited K_t and J_{max} of 4 μM and 0.000413 nmoles/sec/cm^2, respectively, indicating high affinity of estrone sulfate for OAT3. From Fig. 4 and 6 here, estrone sulfate's low K_t would appear to be overestimated by two-fold.

Simulations for Objective 3: Identification of Global Kinetic Conditions when K_t Estimates are Unreliable as a Result of ABL Contribution. The third objective was to identify scenarios under which kinetic estimates are not reliable in spite of ABL consideration, due to ABL dominated transport kinetics. Objective 3 was carried out through simulations incorporating 15% random error, in order to estimate the

probability of successfully estimating K_t. In general, the probability of success increased for progressively lower J_{max} and progressively higher K_t. To a first approximation, the probability of failing to estimate K_t is equal to the percent resistance due to ABL.

These results have implication for the functional characterization and development of QSAR models of transporters. QSAR models rely on kinetic parameters (e.g. J_{max}, K_t, K_i) to relate structural features of substrate/inhibitor to activity. Datasets for QSAR analysis typically comprise kinetic estimates collected across different occasions, including over years and across laboratories. Since transport expression levels vary across occasions, results here imply the quality of kinetic parameter estimates can vary with occasion, if ABL effects are ignored. Biased kinetic parameters underestimate the affinity of potent substrates and overestimate the inhibition potency of modest and poor inhibitors, leading to error in QSAR models.

In summary, our combined data indicate that the ABL resistance layer can have significant impact on carrier-mediated solute transport in over-expression systems. This effect was always observed for hASBT-MDCK, but was most prominent on occasions when J_{max} was high. Failure to consider ABL lead to positively biased estimates of K_t and negatively biased estimates of K_i. The extent of bias is determined collectively by expression level and substrate affinity, such that ABL effect is most prominent for conditions that lead to lowered monolayer resistance (i.e. high J_{max} and low K_t). Results provide three possibilities: (a) Monolayer resistance is sufficiently high (i.e. low J_{max} and high K_t) such that ABL can be ignored and kinetic parameters can be estimated with accuracy and precision; (b) Monolayer resistance is sufficiently high but ABL cannot be ignored for the accurate and precise estimation of kinetic estimates; and (c) Monolayer

JPET Fast Forward. Published on October 12, 2006 as DOI: 10.1124/jpet.106.107433
This article has not been copyedited and formatted. The final version may differ from this version.

resistance for substrate is low (high J_{max} and low K_t) such that flux is highly ABL-controlled, and even consideration of ABL does not allow for accurate and precise estimation of kinetic parameters.

REFERENCES

Adson A, Raub TJ, Burton PS, Barsuhn CL, Hilgers AR, Audus KL and Ho NF (1994) Quantitative approaches to delineate paracellular diffusion in cultured epithelial cell monolayers. *J Pharm Sci* **83**:1529-1536.

Balakrishnan A and Polli JE (2006) Apical sodium dependent bile acid transporter (ASBT, SLC10A2): a potential prodrug target. *Mol Pharm* **3**:223-230.

Balakrishnan A, Sussman DJ and Polli JE (2005) Development of Stably Transfected Monolayer Over-Expressing the Human Apical Sodium-Dependent Bile Acid Transporter (hASBT). *Pharm Res* **22**:1269-1280.

Balakrishnan A, Wring SA and Polli JE (2006) Interaction of native bile acids with human apical sodium-dependent bile acid transporter (hASBT): influence of steroidal hydroxylation pattern and C-24 conjugation. *Pharm Res* **23**:1451-1459.

Ballatori N, Christian WV, Lee JY, Dawson PA, Soroka CJ, Boyer JL, Madejczyk MS and Li N (2005) OSTalpha-OSTbeta: a major basolateral bile acid and steroid transporter in human intestinal, renal, and biliary epithelia. *Hepatology* **42**:1270-1279.

Barry PH and Diamond JM (1984) Effects of unstirred layers on membrane phenomena. *Physiol Rev* **64**:763-872.

Buur A and Mork N (1992) Metabolism of testosterone during in vitro transport across CACO-2 cell monolayers: evidence for beta-hydroxysteroid dehydrogenase activity in differentiated CACO-2 cells. *Pharm Res* **9**:1290-1294.

Dawson PA, Haywood J, Craddock AL, Wilson M, Tietjen M, Kluckman K, Maeda N and Parks JS (2003) Targeted deletion of the ileal bile acid transporter eliminates enterohepatic cycling of bile acids in mice. *J Biol Chem* **278**:33920-33927.

Dawson PA, Hubbert M, Haywood J, Craddock AL, Zerangue N, Christian WV and Ballatori N (2005) The heteromeric organic solute transporter alpha-beta, Ostalpha-Ostbeta, is an ileal basolateral bile acid transporter. *J Biol Chem* **280**:6960-6968.

Herrera-Ruiz D, Faria TN, Bhardwaj RK, Timoszyk J, Gudmundsson OS, Moench P, Wall DA, Smith RL and Knipp GT (2003) A Novel hPepT1 Stably Transfected Cell Line: Establishing a Correlation between Expression and Function. *Mol Pharm* **1**:136-144.

Imanidis G, Waldner C, Mettler C and Leuenberger H (1996) An improved diffusion cell design for determining drug transport parameters across cultured cell monolayers. *J Pharm Sci* **85**:1196-1203.

Polli JW, Wring SA, Humphreys JE, Huang L, Morgan JB, Webster LO and Serabjit-Singh CS (2001) Rational use of in vitro P-glycoprotein assays in drug discovery. *J Pharmacol Exp Ther* **299**:620-628.

Seward DJ, Koh AS, Boyer JL and Ballatori N (2003) Functional complementation between a novel mammalian polygenic transport complex and an evolutionarily ancient organic solute transporter, OSTalpha-OSTbeta. *J Biol Chem* **278**:27473-27482.

Sinko PJ, Leesman GD, Waclawski AP, Yu H and Kou JH (1996) Analysis of intestinal perfusion data for highly permeable drugs using a numerical aqueous resistance--nonlinear regression method. *Pharm Res* **13**:570-576.

Thomson AB (1979) Limitations of the Eadie-Hofstee plot to estimate kinetic parameters of intestinal transport in the presence of an unstirred water layer. *J Membr Biol* **47**:39-57.

Thomson AB and Dietschy JM (1977) Derivation of the equations that describe the effects of unstirred water layers on the kinetic parameters of active transport processes in the intestine. *J Theor Biol* **64**:277-294.

Thomson AB and Dietschy JM (1980) Intestinal kinetic parameters: effects of unstirred layers and transport preparation. *Am J Physiol* **239**:G372-377.

Tolle-Sander S, Lentz KA, Maeda DY, Coop A and Polli JE (2004) Increased acyclovir oral bioavailability via a bile acid conjugate. *Mol Pharm* **1**:40-48.

Visiers I, Weinstein H, Rudnick G and Stephan MM (2003) A Second Site Rescue Mutation Partially Restores Functional Expression to the Serotonin Transporter Mutant V382P. *Biochemistry* **42**:6784-6793.

Winne D (1973) Unstirred layer, source of biased Michaelis constant in membrane transport. *Biochim Biophys Acta* **298**:27-31.

Winne D (1977) Correction of the apparent Michaelis constant, biased by an unstirred layer, if a passive transport component is present. *Biochim Biophys Acta* **464**:118-126.

Winne D (1978) Dependence of intestinal absorption in vivo on the unstirred layer. *Naunyn Schmiedebergs Arch Pharmacol* **304**:175-181.

Winne D, Kopf S and Ulmer ML (1979) Role of unstirred layer in intestinal absorption of phenylalanine in vivo. *Biochim Biophys Acta* **550**:120-130.

Yu H, Cook TJ and Sinko PJ (1997) Evidence for diminished functional expression of intestinal transporters in Caco-2 cell monolayers at high passages. *Pharm Res* **14**:757-762.

Yu H and Sinko PJ (1997) Influence of the microporous substratum and hydrodynamics on resistances to drug transport in cell culture systems: calculation of intrinsic transport parameters. *J Pharm Sci* **86**:1448-1457.

Zhang X, Groves CE, Bahn A, Barendt WM, Prado MD, Rodiger M, Chatsudthipong V, Burckhardt G and Wright SH (2004) Relative contribution of OAT and OCT transporters to organic electrolyte transport in rabbit proximal tubule. *Am J Physiol Renal Physiol* **287**:F999-1010.

Footnotes

[1] Current address: Merck & Co., Inc. West Point, PA19486

This work was support in part by National Institutes of Health grants DK067530 (to JEP) and DK61425 (to PWS).

Address correspondence to: Dr. James E. Polli, Department of Pharmaceutical Sciences, University of Maryland, 20 Penn Street, HSF2 room 623, Baltimore, MD 21201. E-mail : jpolli@rx.umaryland.edu

Legends for Figures

Fig. 1. Plot of taurocholate K_t estimates versus taurocholate J_{max} estimates across different days, using ABL-absent model. There was a strong positive relation between J_{max} and K_t for hASBT-mediated taurocholate flux across hASBT-MDCK monolayers. J_{max} variation can be ascribed to day-to-day variation in hASBT expression. Day-to-day variation in K_t, especially K_t variation that correlates with J_{max}, cannot be explained by the ABL-absent model.

Fig. 2. ABL-absent model and ABL-present model. Panels A and B illustrate the two competing models describing bile acid transport across a hASBT-MDCK monolayer are considered, and are denoted the ABL-absent model and the ABL-present model. Panel C represents the ABL-present model for uptake studies. ABL denotes the aqueous boundary layer (ABL). In panel A, the ABL-absent model is illustrated and only considers monolayer resistance to limit flux, resulting in eqn 1; the resistance due to the support filter and unstirred water layers(s) are considered negligible. Mechanisms of bile acid permeation across the monolayer are active hASBT transport and passive permeability. In panel B, the ABL-present model is illustrated. In eqn 7, the support filter, the apical unstirred water layer, and the basolateral unstirred water layer are collectively denoted as the ABL. In case of uptake studies (Panel C) the term ABL includes only the apical unstirred water layer. The permeability across the ABL is P_{ABL} such that this term represents the permeability across barriers other than the cell monolayer.

Fig. 3. Contour plot showing the effect of ABL on flux for varying J_{max}. The plot describes ABL effect by considering the ratio of J_{ABL} versus J. J_{ABL} is the simulated flux in the ABL-present model (eqn 7), while J is the simulated flux in the ABL-absent model (eqn 1). At the low J_{max} value of 0.00003 nmoles/cm^2/sec, J_{ABL} was generally similar to J (i.e. J_{ABL}/J approximately unity) over all substrate concentrations. At high transporter activity (e.g. J_{max} =0.01 nmoles/cm^2/sec), J_{ABL} was over 10-fold lower than J, particularly for low substrate concentrations. These simulations indicate that ABL resistance is dominant under conditions when monolayer permeability is large (i.e. high J_{max} and low substrate concentration).

Fig. 4. Effect of not considering ABL resistance on K_t estimates. Simulations were performed using eqn 7 (i.e. ABL-present model) over a range of seven J_{max} values, using a K_t of 5 μM. This "true K_t" is illustrated with a broken line. Filled circles indicate K_t estimates from fitting simulated data to eqn 1 (i.e. ABL-absent model). Application of the ABL-absent model generally provided K_t estimates larger than 5 μM. K_t estimates at and below J_{max} of 0.00003 nmoles/cm^2/sec were biased by 0 to 5%. For J_{max} of 0.0003 nmoles/cm^2/sec, the K_t estimate was about 10 μM (i.e. 2-fold higher than true K_t). These results are consistent with experimental taurocholate data where larger K_t estimates were calculated at high J_{max} using the ABL-absent model (i.e Fig. 1).

Fig. 5. Plot of taurocholate K_t estimates versus taurocholate J_{max} estimates across different days, using ABL-present model. In contrast to Fig. 1 where the ABL-absent model was used, there was no dependence of K_t on J_{max} when the ABL-present model

was used. K_t was practically the same (about 8 μM) across different days, as expected. K_t estimates from the ABL-present model were about 3-fold lower than K_t estimates from the ABL-absent model, consistent with the simulations in Fig. 4.

Fig. 6. Interplay of J_{max} and K_t in determining the impact of ABL on flux. J_{ABL} and J were simulated using the ABL-present and ABL-absent models, respectively, over a range of J_{max} and K_t. The combination of J and K_t significantly determined the role of ABL on flux. When J_{max} was very low, ABL is only significant when K_t is very low. For progressively higher J_{max}, ABL is significant for a wider range of K_t values. The effect of ABL is most prominent for conditions that allow for high monolayer permeability (i.e. high J_{max} and low K_t), such that J_{ABL} is 10-fold lower than J.

Fig. 7. Contour plot showing the effect of ABL on flux in the presence of inhibitor for varying J_{max}. The plot describes ABL effect by considering the ratio of J_{ABL} versus J. Simulations were performed using S = 2.5 μM, K_t = 5 μM, $P_p = 0.5x10^{-6}$ cm/s, and K_i = 5 μM. The contour plot indicates that the interplay of J_{max} and inhibitor concentration can collectively limit the effective monolayer permeability and hence the contribution of ABL in overall resistance to flux. At the low J_{max} value of 0.00003 nmoles/cm^2/sec, J_{ABL} was generally similar to J over all inhibitor concentrations. At high transporter activity (e.g. J_{max} =0.01 nmole/cm^2/sec), J_{ABL} was significantly lower than J, particularly for low inhibitor concentrations. These simulations indicate that ABL resistance is dominant under conditions when monolayer permeability is high (i.e. high J_{max} and low inhibitor concentration).

Fig. 8. Effect of not considering ABL resistance on K_i estimates. Simulations were performed using eqn 11 (i.e. ABL-present model for inhibition) over a range of six J_{max} values, using a K_t of 5 μM and K_i of 50 μM. This "true K_i" is illustrated with a broken line. Filled circles indicate K_i estimates from fitting simulated data to eqn 10 (i.e. ABL-absent model for inhibition). Application of the ABL-absent model generally provided K_i estimates lower than 5 μM. Qualitatively, this negative bias is opposite the positive bias observed in Fig. 4 for K_t, although both simulations indicate ABL to limit substrate flux. K_i estimates at and below J_{max} of 0.00001 nmoles/cm^2/sec were biased by 0 to 10%. For J_{max} of 0.0003 nmole/cm^2/sec, the K_i estimate was about 10 μM (i.e. over 5-fold lower than true K_i).

Fig. 9. Interplay of J_{max} and K_t in determining ABL impact on K_i estimate. Error-free data were generated via the ABL-present transport inhibition model (i.e. eqn 11) over a range of substrate K_t values and J_{max} values, using a "true K_i" of 50 μM. This "true K_i" is illustrated as a broken line. Data were subsequently fit to the ABL-absent inhibition model (i.e. eqn 10), with the estimated K_i values plotted. In all cases, K_i estimates were negatively biased, particularly for low K_t values, regardless of J_{max}.

Fig. 10. hASBT expression level and J_{max}. Panels A shows Western blot analysis of hASBT expressed at cell surface. MDCK cells stably transfected with hASBT construct were treated with 10 mM sodium butyrate (A), 5 mM sodium butyrate (B), or no sodium butyrate treatment (C). Untransfected MDCK cells are also shown (D) and did not

receive any sodium butyrate treatments. Molecular weight marker lanes (M) are depicted to the left of the blots. hASBT-MDCK cells were incubated with sulfo-NHS-SS-biotin as described under Materials and Methods. Western blots were probed with anti-V5/HRP antibody (1:1000 dilution) directed to the hASBT/V5 construct. The 41 kDa band represents mature, glycosylated hASBT; the 150 kDa band is the biotinylated control marker α-integrin, a constitutively expressed plasma membrane protein. In Panel B, J_{max} values from the hASBT-MDCK monolayers treated with the three different levels of sodium butyrate showed a linear relationship with band density using pixel intensity (r^2 = 0.994 with slope = 6.17×10^{-4} nmole/sec/cm^2 and intercept = -0.764×10^{-4} nmole/sec/cm^2). Pixel intensity analysis employed NIH Image software and normalized hASBT band pixel intensity against and α-integrin band pixel intensity, after correction for background control (lane D).

Table 1 ABL influence on taurocholate inhibition kinetics. Taurocholate K_i values were calculated using both the ABL-present inhibition model and the ABL-absent inhibition model. As expected from simulation results (Fig. 8 and 9), K_i values from ABL-absent inhibition model was always lower than the K_i estimates from ABL-present inhibition model.

Occasion	Taurocholate K_i values (μM)	
	ABL-absent inhibition model	ABL-present inhibition model
1	1.45 (±0.21)	2.88 (±0.25)
2	1.25 (±0.30)	4.10 (±0.32)
3	2.78 (±0.53)	8.30 (±0.64)
4	0.65 (±0.22)	1.22 (±0.10)
5	3.35 (±0.76)	12.11 (±0.60)
6	0.90 (±0.18)	1.69 (±0.09)
7	4.09 (±0.26)	5.56 (±0.24)
8	2.10 (±0.09)	2.63 (±0.16)
9	4.67 (±0.32)	6.43 (±0.36)
10	0.30 (±0.22)	2.07 (±0.11)
11	0.69 (±0.30)	2.91 (±0.13)
12	3.96 (±0.42)	6.33 (±0.25)

Values are the average of three observations (± SEM).

JPET Fast Forward. Published on October 12, 2006 as DOI: 10.1124/jpet.106.107433
This article has not been copyedited and formatted. The final version may differ from this version.

Table 2 Probability of obtaining statistically significant K_t estimate under different scenarios of K_t and J_{max}. K_t was estimated on 100 occasions for each scenario using simulated data that incorporated 15% random error. The probability of successful K_t estimation was the percent of occasions when the 95% confidence interval for K_t did not include zero. Tabulated in parenthesis is the percent of total resistance due to ABL (percent ABL resistance). When J_{max} is high, probability of successful K_t estimation was low, especially when true K_t was less than 10 μM. At progressively lower J_{max}, the chance of successful K_t estimation improved. For most of the scenarios evaluated, the probability of successful K_t estimation depended on the contribution of ABL resistance to flux (i.e. percent ABL resistance); when flux became increasingly ABL-limited, chances of success decreased.

K_t (μM)	Probability of Successful K_t Estimation (*percent ABL resistance*)		
	J_{max} (nmoles/cm^2/sec)		
	0.001	0.0003	0.0001
1	10% (*94%*)	13% (*81%*)	65% (*59%*)
3	19% (*83%*)	58% (*59%*)	90% (*32%*)
5	43% (*74%*)	79% (*46%*)	91% (*15%*)
10	59% (*58%*)	92% (*30%*)	84% (*12%*)
25	87% (*36%*)	86% (*15%*)	64% (*5%*)

Figure 1

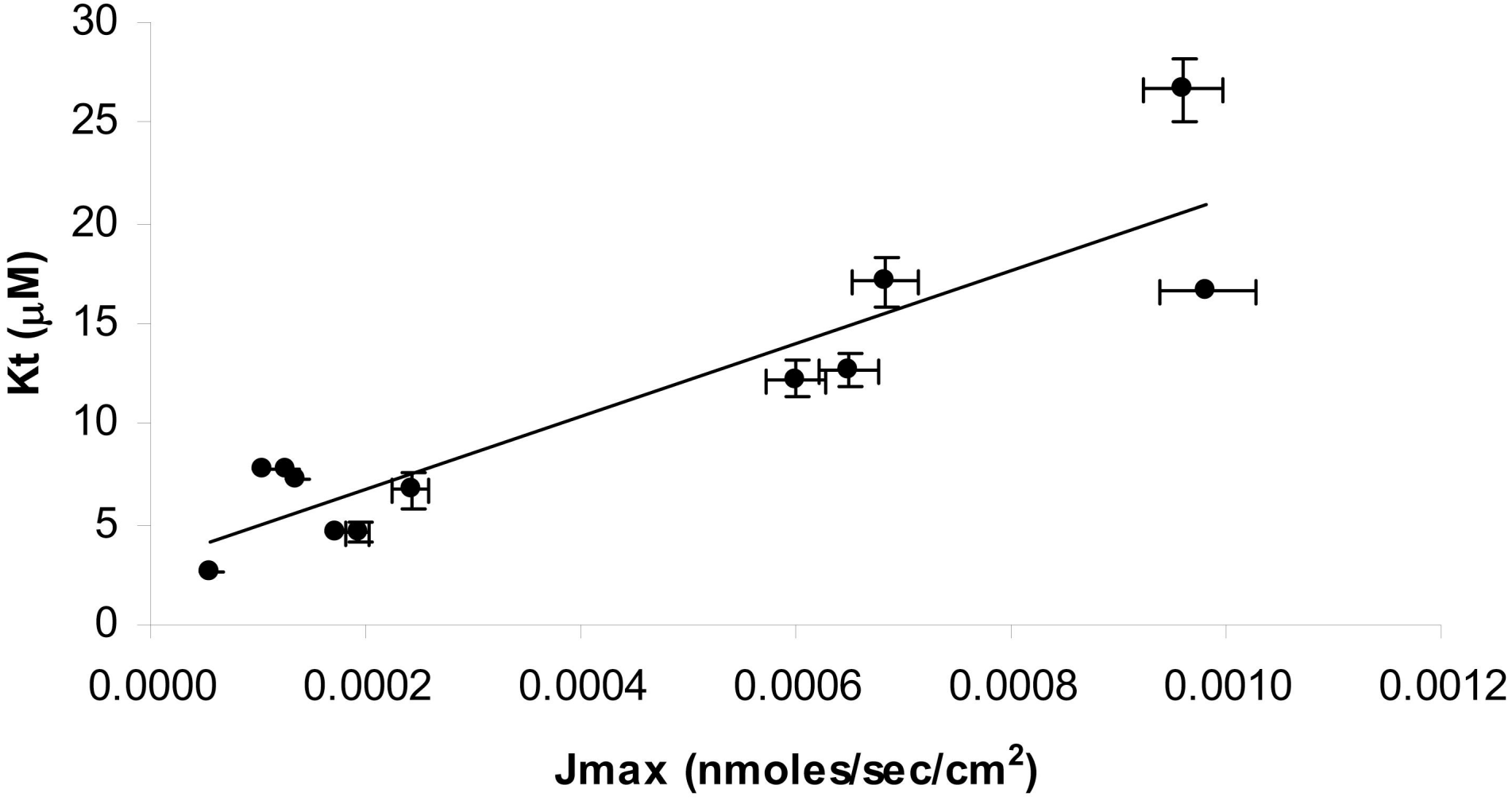
30
25
20
15
10
5
0
Kt (μM)
0.0000
0.0002
0.0004
0.0006
0.0008
0.0010
0.0012
Jmax (nmoles/sec/cm2)

Figure 2

Panel A

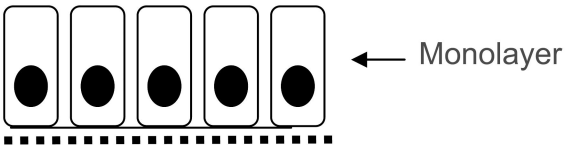

Panel B

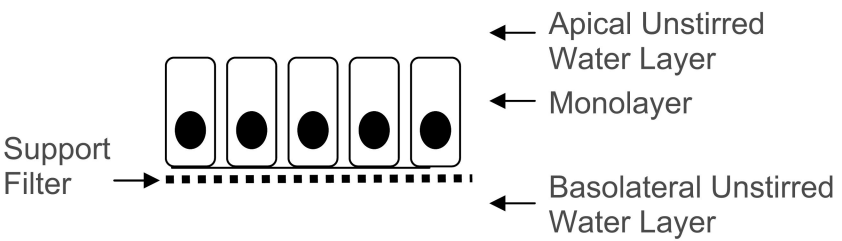

Panel C

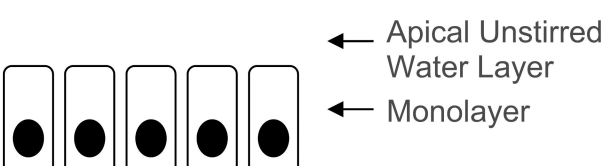

Figure 3

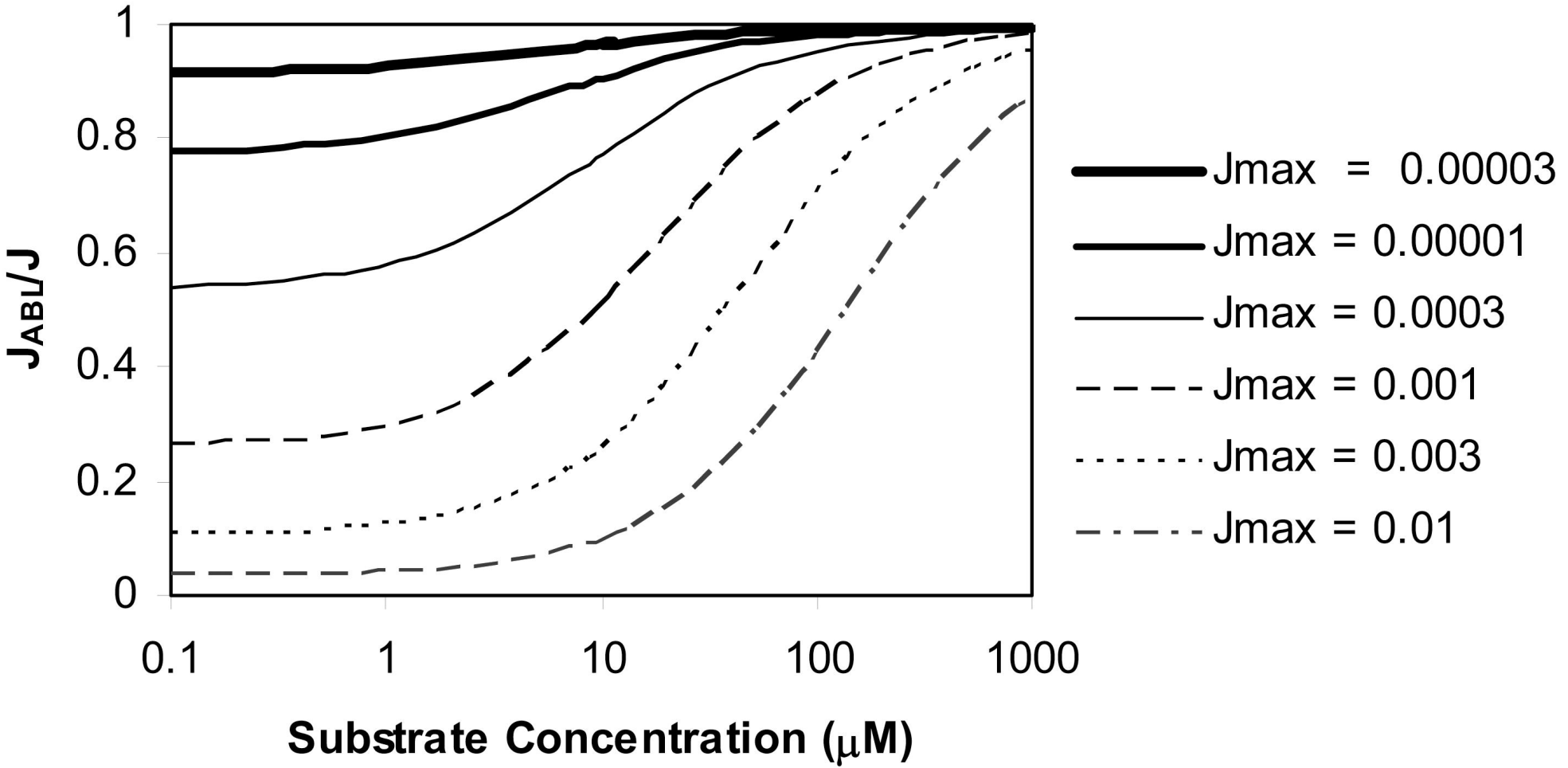
1
0.8
0.6
0.4
0.2
0
J_{ABL}/J
0.1
1
10
100
1000
Substrate Concentration (μM)
Jmax = 0.00003
Jmax = 0.00001
Jmax = 0.0003
Jmax = 0.001
Jmax = 0.003
Jmax = 0.01

Figure 4

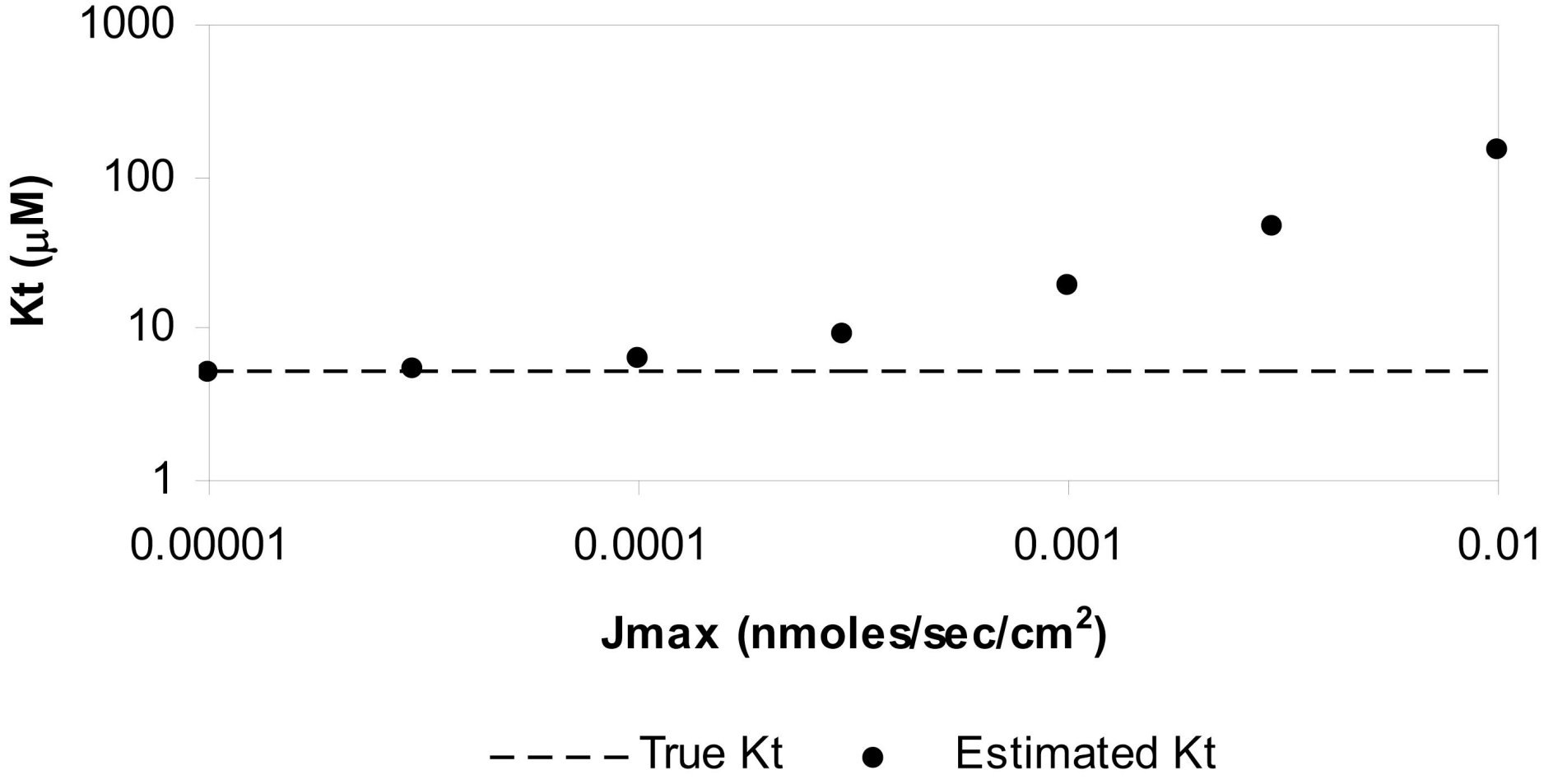
1000
100
10
1
Kt (μM)
0.00001
0.0001
0.001
0.01
Jmax (nmoles/sec/cm2)
True Kt
Estimated Kt

Figure 5

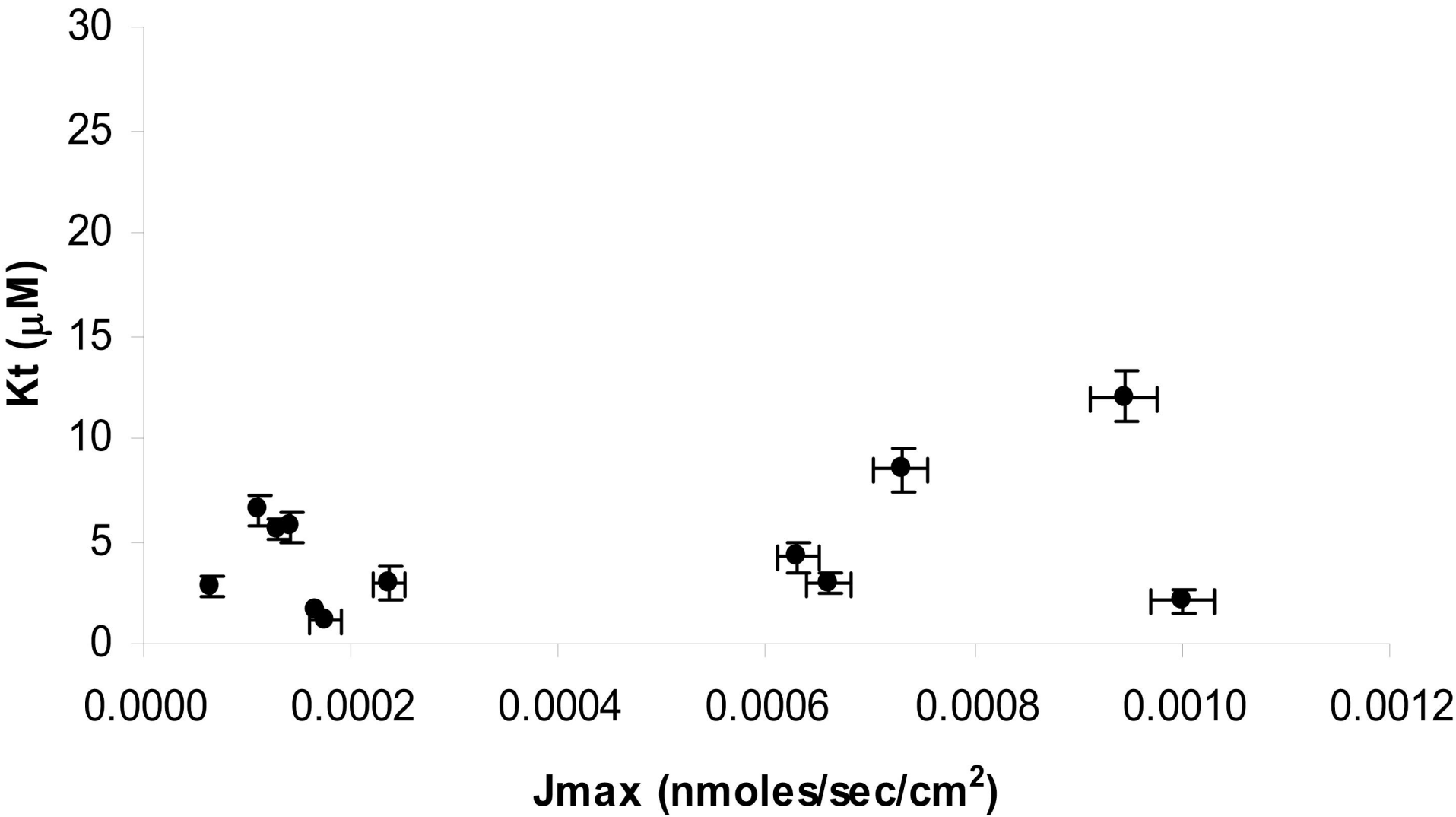
30
25
20
15
10
5
0
Kt (μM)
0.0000
0.0002
0.0004
0.0006
0.0008
0.0010
0.0012
Jmax (nmoles/sec/cm2)

Figure 6

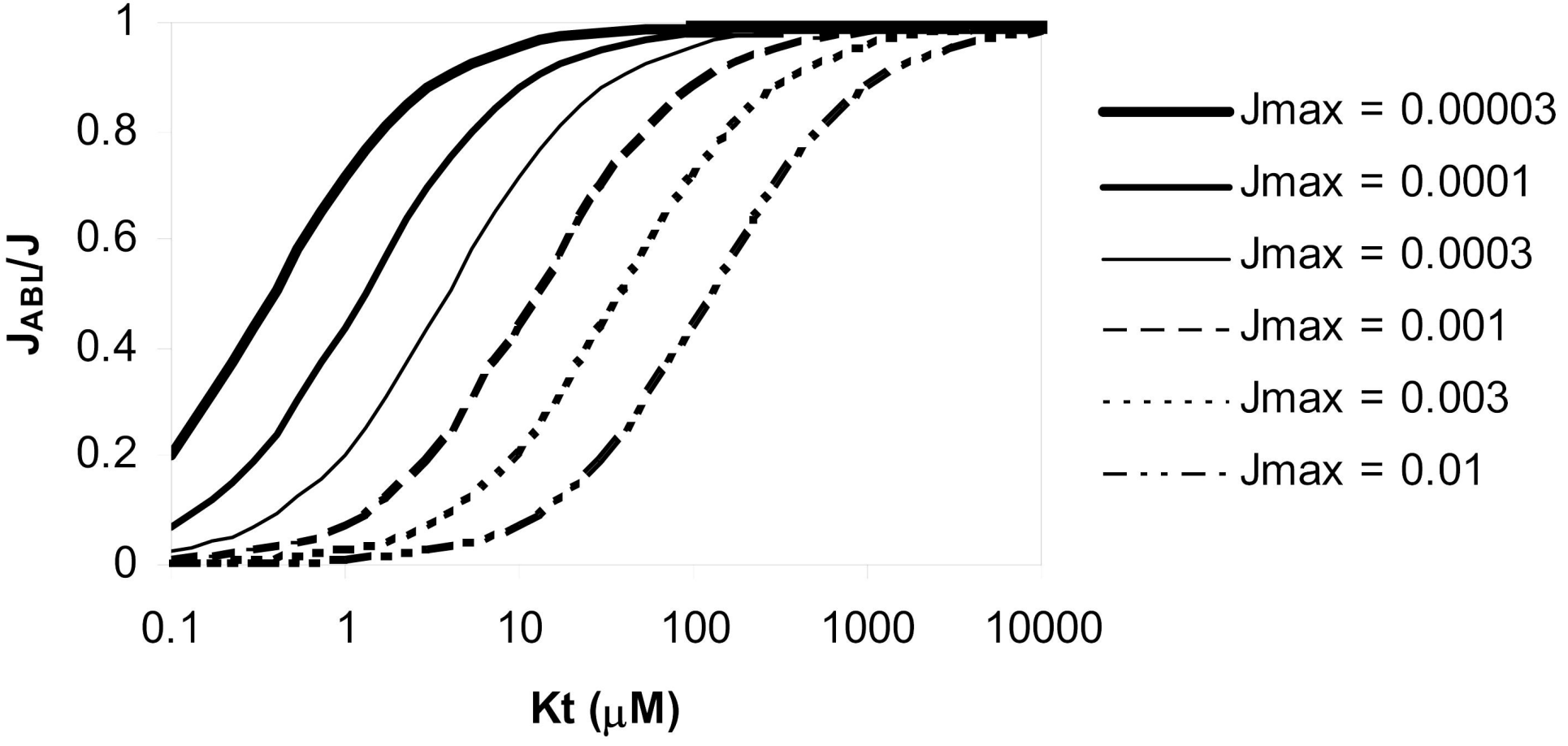
1
0.8
0.6
0.4
0.2
0
J_{ABL}/J
0.1
1
10
100
1000
10000
Kt (μM)
Jmax = 0.00003
Jmax = 0.0001
Jmax = 0.0003
Jmax = 0.001
Jmax = 0.003
Jmax = 0.01

Figure 7

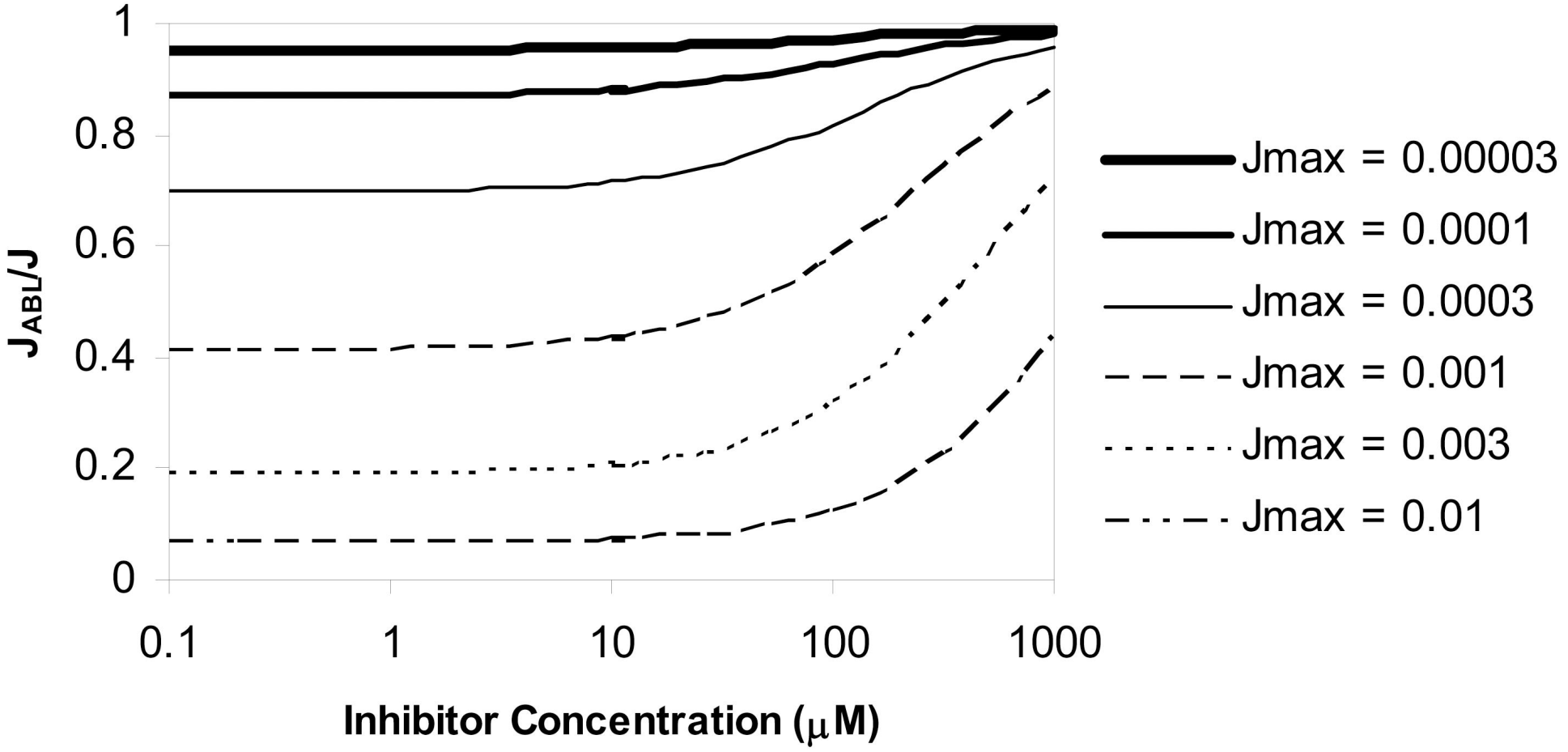
1
0.8
0.6
0.4
0.2
0
J_{ABL}/J
0.1
1
10
100
1000
Inhibitor Concentration (μM)
Jmax = 0.00003
Jmax = 0.0001
Jmax = 0.0003
Jmax = 0.001
Jmax = 0.003
Jmax = 0.01

Figure 8

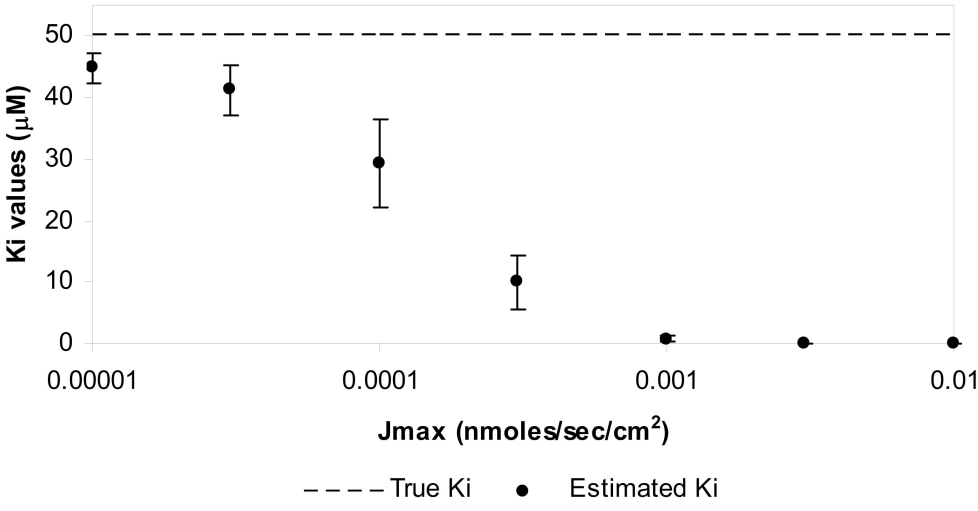
50
40
30
20
10
0
Ki values (μM)
0.00001
0.0001
0.001
0.01
Jmax (nmoles/sec/cm2)
True Ki
Estimated Ki

Figure 9

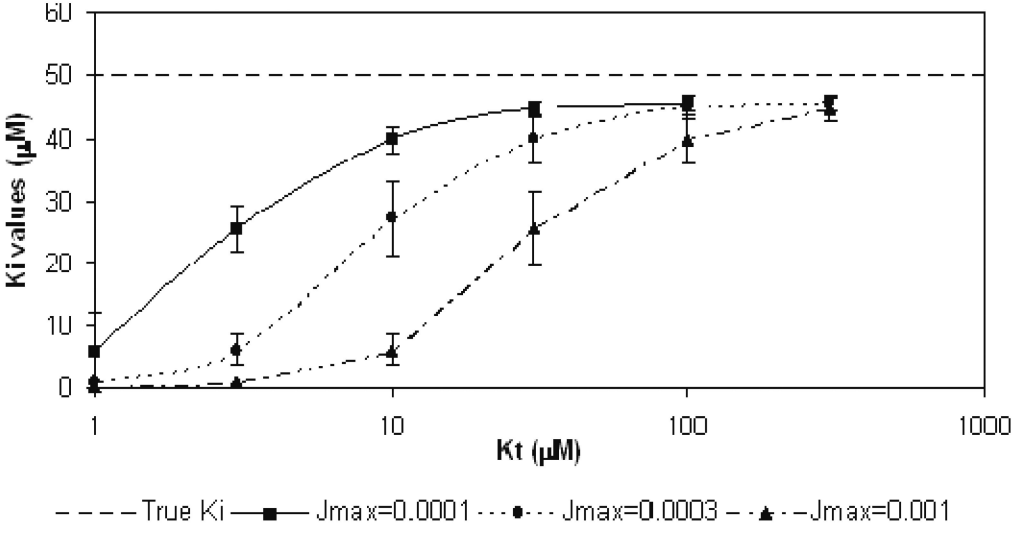
60
50
40
30
20
10
0
Ki values (μM)
1
10
100
1000
Kt (μM)
True Ki
Jmax=0.0001
Jmax=0.0003
Jmax=0.001

Figure 10

Panel A

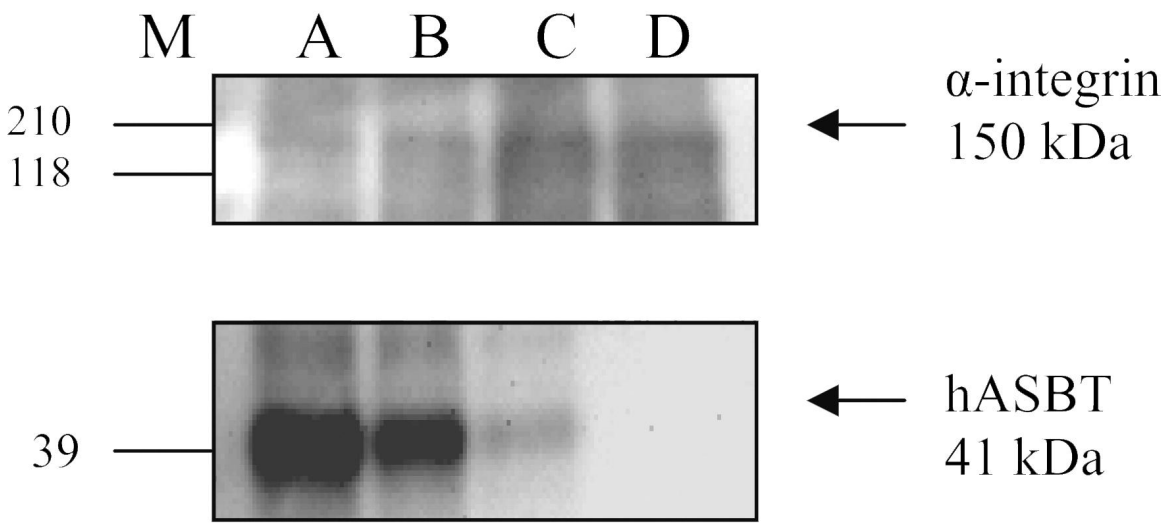

Panel B

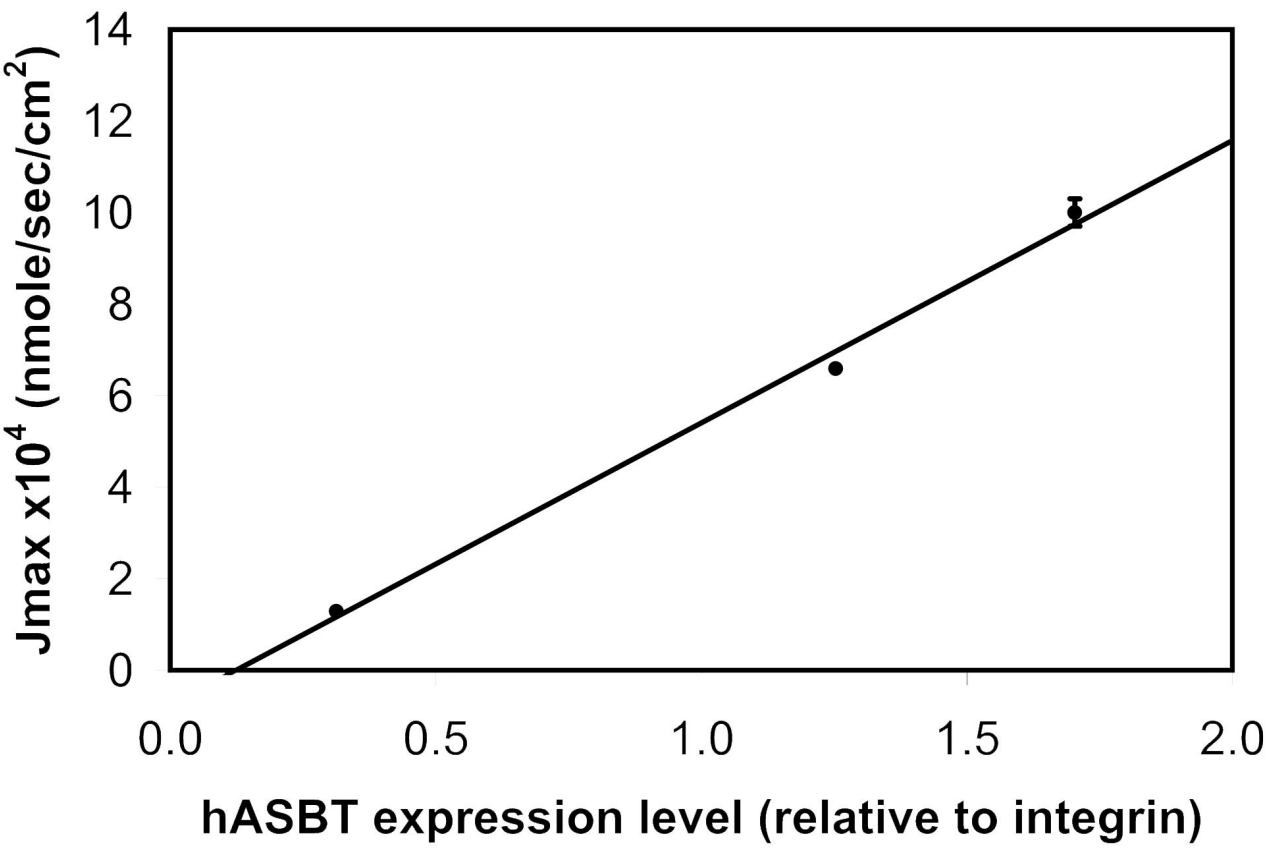

JPET Fast Forward. Published on October 12, 2006 as DOI: 10.1124/jpet.106.107433
This article has not been copyedited and formatted. The final version may differ from this version.

APPENDIX 1

The objective of Appendix 1 is to derive eqn 9. For the ABL-present model:

$$R_{app} = R_{ABL} + R_{mono} \qquad \text{(A1)}$$

Hence, in comparing the relative resistances in the ABL-absent model and the ABL-present model,

$$F_{mono} = \frac{R_{mono}}{R_{mono} + R_{ABL}} \qquad \text{(A2)}$$

where F_{mono} is the fraction of total flux resistance that is due to the monolayer.

$$F_{mono} = \frac{1/P_{mono}}{1/P_{app}} \qquad \text{(A3)}$$

$$F_{mono} = \frac{S/J}{S/J_{ABL}} \qquad \text{(A4)}$$

$$F_{mono} = \frac{J_{ABL}}{J} \qquad \text{(A5)}$$

JPET Fast Forward. Published on October 12, 2006 as DOI: 10.1124/jpet.106.107433
This article has not been copyedited and formatted. The final version may differ from this version.

APPENDIX 2

The objective of Appendix 2 is to derive the ABL-present inhibition model (i.e. eqn 11).

Substrate flux in the presence of an inhibitor when ABL is absent is described by

$$J = \frac{J_{\max} \cdot S}{K_t\left(1 + I/K_i\right) + S} + P_p \cdot S \qquad \text{(A6)}$$

where I is the concentration of inhibitor (i.e. inhibitory bile acid) and K_i is inhibitory constant. S is substrate concentration (i.e. taurocholate concentration); J_{max}, K_t, and Pp characterize substrate transport parameters.

In the ABL-present model, since permeability is the inverse of resistance:

$$\frac{1}{P_{app}} = \frac{1}{P_{ABL}} + \frac{1}{P_{mono}} \qquad \text{(A7)}$$

where P_{app} is the apparent permeability, P_{ABL} is the ABL permeability, and P_{mono} is the monolayer permeability.

From eqn A6, monolayer permeability in the presence of inhibitor is

$$P_{mono} = \frac{J_{\max}}{K_t\left(1 + I/K_i\right) + S} + P_p \qquad \text{(A8)}$$

Substituting eqn A8 into eqn A7,

$$\frac{1}{P_{app}} = \frac{1}{P_{ABL}} + \frac{1}{\dfrac{J_{\max}}{K_t\left(1 + I/K_i\right) + S} + P_p} \qquad \text{(A9)}$$

JPET Fast Forward. Published on October 12, 2006 as DOI: 10.1124/jpet.106.107433
This article has not been copyedited and formatted. The final version may differ from this version.

$$P_{app} = \frac{P_{ABL} \cdot \left(\frac{J_{\max}}{K_t\left(1 + I/K_i\right) + S} + P_p \right)}{P_{ABL} + \frac{J_{\max}}{K_t\left(1 + I/K_i\right) + S} + P_p} \qquad \text{(A10)}$$

Since $J_{ABL} = P_{app} \cdot S$,

$$J_{ABL} = \frac{P_{ABL} \cdot \left(\frac{J_{\max}}{K_t\left(1 + I/K_i\right) + S} + P_p \right) \cdot S}{P_{ABL} + \frac{J_{\max}}{K_t\left(1 + I/K_i\right) + S} + P_p} \qquad \text{(A11)}$$

APPENDIX 3

The objectives of Appendix 3 are to a) provide support for the presumption that, in Fig. 1, variation in Jmax can be ascribed to variation in hASBT expression and b) provide further support that ABL influence is modulated by Jmax. Figure 1 inspired the hypothesis that high transporter expression can lower monolayer resistance, resulting in ABL-limited transport of solutes, leading to biased kinetic estimates if ABL is not considered.

Figure 10 shows Western blot analysis of hASBT expressed at cell surface (Panel A), as well as correlation between measure J_{max} and hASBT expression level (relative to integrin) (Panel B). In Panel A, Western blots were consistent with expected results, where hASBT expression decreased in the following order: lane A (hASBT-MDCK treated with 10 mM sodium butyrate) < lane B (hASBT-MDCK treated with 5 mM sodium butyrate) < lane C (hASBT-MDCK treated with no sodium butyrate) < lane D (untransfected MDCK). In Panel B, hASBT expression level from band density analysis using pixel intensity provided linear association (r^2=0.994) with measured taurocholate J_{max} values, which were 10.0(±0.3) x 10^{-4} nmoles/cm^2/sec, 6.59(±0.21) x 10^{-4} nmoles/cm^2/sec, and 1.29(±0.05) x 10^{-4} nmoles/cm^2/sec for lanes A, B, and C, respectively. Untransfected MDCK (lane D) showed no active taurocholate flux. Hence, variation in J_{max} was attributable to variation in hASBT expression at cell surface. A similar analysis was performed by Irie et al., where PEPT1 mRNA level was linearly associated with Gly-Sar J_{max} values (r = 0.55) across Caco-2 clones (Irie et al., 2006).

As expected, when ABL-influence was not considered, the K_t estimates were positively association with Jmax; K_t values were 19.6(±2.4), 15.3(±1.72) and 7.47(±0.50)

μM for lanes A, B, and C, respectively. When the ABL-present model was applied to this same data, this association was abolished; K_t values were 3.24(±1.01), 3.73(±0.70), 5.77(±0.40) μM for lanes A, B, and C, respectively. Result here from hASBT-MDCK monolayers subjected to differing levels of induction by sodium butyrate provide further support that ABL influence is modulated by Jmax.

JPET Fast Forward. Published on October 12, 2006 as DOI: 10.1124/jpet.106.107433
This article has not been copyedited and formatted. The final version may differ from this version.

APPENDIX 4

The objective of Appendix 4 is to evaluate the ability of the ABL-present model to accurately estimate kinetic parameter estimates from uptake studies (i.e. J_{max}, K_t), relative to the Winne uptake model. Taurocholate uptake data from five occasions were regressed onto eqn 7 and 8 using SigmaPlot2000 (SPSS Inc.; Chicago, IL). Kinetic parameters were compared via the paired t-test.

This comparison is motivated since Winne's uptake model is tailored for uptake configuration. Winne's uptake model would appear not be applicable to transport studies, by virtue of its high identifiability as an uptake model. Favorable performance of the ABL-present model in assessing uptake data, compared to the Winne uptake model, would support the ABL-present model to serve as a single form to analyze both transport and uptake data that require ABL consideration.

For each occasion, J_{max} and K_t values from the ABL-present model were statistically indistinguishable from J_{max} and K_t values from the Winne uptake model ($p>0.05$). Additionally, the ABL-present model effectively eliminated the bias in K_t that otherwise results from ABL. As was observed from transport studies in Fig. 1, there was a positive, linear association between K_t and J_{max}, when the ABL-absent model was applied to uptake data ($r^2=0.79$). Application of the ABL-present model markedly attenuated the association ($r^2=0.08$), as did the Winne uptake model.

Favorable performance of the ABL-present model in assessing uptake data supports the ABL-present model to serve as a single form to analyze both transport and uptake data that require ABL consideration.